INTERACTIVE CONTROL ENGINEERING
Principles and Applications

Volume 20 Motion Control, Robotics, and Autonomous Systems

CHAPTER 7

CubeSat Attitude Simulator Whose Wheels Keep Every Torque They Absorb

Pages 158–186

Edited by John D. Hedengren

How to cite this chapter. "CubeSat Attitude Simulator Whose Wheels Keep Every Torque They Absorb," in *Motion Control, Robotics, and Autonomous Systems*, John D. Hedengren, Ed., vol. 20 of *Interactive Control Engineering: Principles and Applications*. Advanced Process Solutions, LLC, 2026, ch. 7, pp. 158–186.

The page numbers in this file are those of the printed volume.

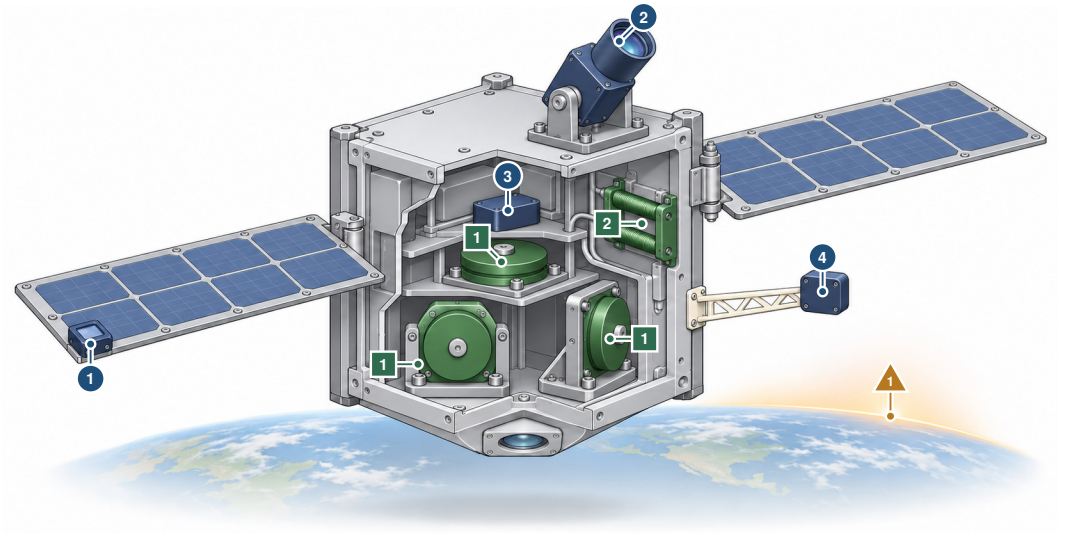
The app for this chapter
https://apmonitor.com/apps/satellite-attitude/

The volume online: contents, other chapters and citation records
https://apmonitor.com/apps/books/v20-motion-robotics/#satellite-attitude

Copyright © 2026 Advanced Process Solutions, LLC. All rights reserved. Produced by Advanced Process Solutions, LLC.

CHAPTER 7

CubeSat Attitude Simulator Whose Wheels Keep Every Torque They Absorb



The controller moves 1 three reaction wheels, one on each axis 2 magnetic torque coils

The controller reads 1 sun sensor on a solar array 2 star tracker, looking away from the Earth 3 gyro 4 magnetometer on a short boom

What disturbs it 1 the Sun, which blinds the star tracker when it comes near its line of sight

Notice the camera window facing the Earth and the star tracker looking the other way, while the wheels inside can turn the satellite but keep every push they absorb. Illustration, not to scale.

IN PLAIN TERMS Pointing a Small Satellite With Spinning Wheels

The main idea. A small satellite turns its camera by spinning little wheels inside it the other way, as a person on a free office chair turns by swinging an arm. Magnetic coils push on the Earth's field to slow the wheels again.

The challenge. The wheels soak up every push of the thin air until they spin their fastest, and the coils push only across the Earth's field. The star camera that shows where the satellite points goes blind when the Sun shines into it.

Why it matters. Sharing the work between wheels, coils and the best guess of where the satellite points decides whether the camera holds its spot on the ground.

THREE WAYS TO READ THIS CHAPTER

Explore	12 min	the first page, the fact in the Introduction, the two history segments of Section 7.2, the try-it segments of scenarios 3 and 6 and the fact on the challenge (Section 7.6), and the key points
Study	60 min	the whole chapter with its three pause points and the twelve exercises at its end
Practice	20 min	the first page, the measured cases (Section 7.6), Technology in Practice (Section 7.7), Limitations (Section 7.8) and the open challenge

The control question Reaction wheels turn a small satellite but keep every torque they absorb, and magnetic coils can empty them only across the Earth's field. How must pointing, momentum unloading and attitude estimation share the work so that the camera still holds a ground site through a pass with its star tracker half blind?

Learning objectives

- Compute how fast a constant disturbance torque fills a reaction wheel, and explain why no pointing gain changes it.
- Predict the orbit-averaged unloading rates of the cross-product law from the field's direction, and explain why a strong B-dot gain detumbles slowly.
- Compare an eigenaxis slew with three single-axis loops by the angle turned and the peak body rate.
- Explain why an attitude filter carries the gyro bias as a state, and measure what leaving it out costs during a blind window.
- Judge what a predictive pointing law adds on a handover: the limits it keeps rather than its preview.

Prerequisites Sections 1.4.2 (eigenaxis and stored momentum), 1.4.6 (bias state), 1.4.7 (directional actuators) and 1.6.4 (scenarios and the scorecard). Section 1.6.3 is needed only for the predictive law.

The app https://apmonitor.com/apps/satellite-attitude/

See also Volume 4: Volume 4, Chapter 13 for actuators that push only inside a cone and Volume 4, Chapter 12 for allocation against a consumable budget. Volume 5: Volume 5, Chapter 13 for drift between position fixes and Volume 5, Chapter 12 for a store that is never measured.

7.1 Introduction

An Earth-observation satellite the size of a shoebox now carries the same kinds of actuators and sensors as a large one. The CubeSat standard fixed the outside of such a spacecraft and its interface to a shared deployer, so that many of them could ride as secondary payloads and share a development cost [1], and a 3U CubeSat designed in 2019 was to point better than 0.25° with reaction wheels and a star tracker, its attitude filter running on a microcontroller [2]. Those actuators behave unlike a valve or a heater. A reaction wheel turns the body by spinning the other way, so it moves angular momentum between itself and the spacecraft and removes none of it, and a magnetorquer coil feels a torque $\mathbf{m} \times \mathbf{B}$ that is always perpendicular to the local field. The physics is textbook material, with sensors and actuators, attitude filtering and attitude control each given a chapter of a standard text [3], but its consequences for a controller are easy to miss.

> ✦ DID YOU KNOW? **Despun by the Field in Two Years**
>
> Eddy currents that the Earth's magnetic field drove in the spinning outer shell of Vanguard I slowed it from 2.7 revolutions a second at launch to less than 0.2 revolutions a second two years later [4]. The coils of this chapter use the same field on purpose, to unload the wheels.

Intuition carried over from process loops misleads on this plant, and the simulator puts a number on each surprise. A wheel controller that holds the camera within a few hundredths of a degree looks able to hold it indefinitely, yet at nadir a drag torque of 2 µN m, fixed in the body about pitch, fills the pitch wheel by 37.85 % of its capacity every orbit, and after 245.0 min that wheel can absorb nothing more and the attitude is lost. A stronger magnetic law looks faster, yet B-dot at 8 mN m s needs 85.5 min to bring a 10.1 °/s tumble under 0.5 °/s where 0.5 mN m s needs 26.8, because the strong law leaves the spacecraft turning about the field line, where no coil has any authority. An attitude held on its setpoint looks like an attitude achieved, yet while the Sun blinds the star tracker for 11.6 min a filter that leaves out the gyro bias lets the camera drift 2.35° from nadir, with the pointing loop holding its own estimate on nadir throughout. The double integrator $1/(Js^2)$ from wheel torque to angle contains none of this, because the storage, the direction of the field and the estimate all lie outside it.

None of the three is peculiar to spacecraft. An actuator that stores what it applies needs a second actuator to unload it, and the unloading becomes a slow loop sized against the secular disturbances, which for magnetic laws has been analyzed by averaging their effect over an orbit [5]. Magnetic actuation adds a control direction that the orbit keeps turning, which makes pointing with coils alone a time-varying problem, although it has been shown to have global solutions by attitude and rate feedback [6], and detumbling with coils alone has a convergence proof and a gain criterion that allows for saturated coils [7]. A walking robot meets the same restriction in feet that push only inside a friction cone (Volume 4, Chapter 13). The estimation half integrates a biased rate sensor between absolute fixes that come and go, the arrangement in which the gyro bias became a state of attitude filters [8], and the one in which an underwater vehicle drifts between acoustic fixes (Volume 5, Chapter 13). A surge drum under averaging level control shares the first half of this shape, storing every flow imbalance until a slower loop returns the inventory.

The literature studies these pieces apart, the unloading law by its orbit average [5], the magnetic laws by their convergence [6, 7] and the filter by its error representation [9]. This chapter puts them on one browser simulator of a 6U CubeSat whose flight software sees only its instruments. On it the wheels can be watched filling, the momentum beyond the coils' reach can be read at every instant, and one orbit can be flown with and without the gyro bias in the filter, so that pointing, stored momentum and imaged pass can be apportioned among the layers of an attitude control system. Quaternion feedback, B-dot, the cross-product unloading law and the multiplicative filter are standard laws taken from the literature. Two predictions check the engine, the orbit-averaged unloading rates, under which a pitch excess falls to a tenth in 36.2 min against a predicted 35.1 and an excess in the orbit plane in 64.4 to 70.3 min against 67.9 to 68.1, and the gravity-gradient libration of the free spacecraft, 84.65 min against 84.63. The spacecraft has ten states with its orbit, Sun, shadow and field, instruments that are the controller's only view of the truth, two filters fed the same readings in parallel and a mode supervisor, written down completely enough to be rebuilt. Ten cases and a challenge isolate storage, field geometry, slewing, estimation, an honestly infeasible wheel failure and a handover slewed by an optional model predictive controller, whose measured comparison with the shipped laws credits it with the limits it keeps rather than with speed.

Section 7.2 traces how spacecraft came to be pointed. Section 7.3 sets out the spacecraft, its orbit and its instruments, and Section 7.4 what the inertia and the field permit any controller. Section 7.5 describes the flight software, with the predictive law in Section 7.5.5. Section 7.6 measures the ten cases and the challenge, and Section 7.6.11 sets the predictive law beside the shipped laws. Section 7.7 names the devices of real spacecraft, Section 7.8 states the limitations and Section 7.9 draws the lessons together. The background comes from Chapter 1: the eigenaxis and the momentum stored in wheels from Section 1.4.2, the bias state from Section 1.4.6, actuators that act in only some directions from Section 1.4.7, and the simulator framework from Section 1.6.

7.2 From Spinning Satellites to Three-Axis CubeSats

A spinning body keeps its axis fixed in space, but its environment wears the spin down and moves the axis, as the history box below tells for the first satellites that met the Earth's field. A report of 1961 from the Applied Physics Laboratory set out how the attitude of an Earth satellite could be stabilized by magnetic and by gravity torques, and how the attitude acts on the solar power and the thermal balance [10]. By 1978 attitude determination, prediction and control had grown into a reference of 858 pages prepared by the Computer Sciences Corporation, whose foreword, from the head of the attitude section at NASA's Goddard Space Flight Center, explained that comprehensive reference material had been difficult to obtain [11].

HISTORY The Field as Disturbance and as Tool (1962 to 1969)

In the weather satellite Tiros I, a large magnetic dipole inside the spacecraft turned against the Earth's field, precessed the spin axis and changed the direction of the cameras in ways nobody had predicted. Designers soon used the same torques on purpose. Transit 1B carried a permanent magnet to hold its axis along the local field, and later Tiros satellites aimed their cameras by changing their magnetic moment on command from the ground [4]. On the spin-stabilized Telstar satellite of 1962, eddy-current and magnetic torques slowed the spin with a characteristic time estimated at about 330 days and drifted the spin axis, while a damper cut the precession angle by a factor of e within 30 min at most [12].

Active magnetic control used the same field. An elementary magnetic attitude control system was published in 1976 [13]. Inertial pointing with coils alone was shown in 2002 to have a global solution by static attitude and rate feedback and by dynamic attitude feedback [6], and a rigorous proof that coils alone bring a rigid spacecraft to rest from arbitrary tumbling in a time-varying field came in 2012, together with a simple criterion for a gain that detumbles in quasi-minimum time while the coils saturate [7].

Reaction wheels gave three-axis control without propellant and created the problem of unloading them. Analytical formulas for the orbit-averaged behavior of magnetic laws that unload a reaction wheel system against secular environmental torques were derived in 1980 for an inertially fixed spacecraft whose dominant disturbance was the gravity gradient, and they agreed within 10 % with detailed simulations of the Solar Maximum Mission spacecraft [5]. Section 7.4 applies the same averaging to the Earth-pointing spacecraft of the simulator.

Large slews came to be flown on quaternion errors. The stability of large-angle reorientations under quaternion feedback, with a strapdown inertial reference supplying the attitude change and reaction jets under pulse-width pulse-frequency modulation supplying nearly proportional torques, was analyzed with Liapunov's theorem in 1985 [14], and a quaternion feedback regulator for rotations about the eigenaxis followed in 1989 [15]. Attitude knowledge took a parallel path. A review of 1982 gathered the Kalman filters for spacecraft that carry three-axis gyros and attitude sensors, in which the gyro data replace a dynamic model, the attitude state is augmented with the gyro biases, and the gyro noise enters as state noise rather than as observation noise [8]. Because the quaternion must keep a unit norm, the filter keeps a quaternion for the global attitude and a three-component representation for its error, the form called the multiplicative extended Kalman filter [9]. One absolute reference for such a filter is the autonomous star tracker, an electronic camera whose processor identifies stars against an internal catalog and computes the attitude quaternion by itself [16].

The CubeSat brought these pieces to small spacecraft. A standard deployer developed with Cal Poly students was designed to release CubeSats as secondary payloads on a wide range of launchers, provided each conformed to common physical requirements and shared the deployer interface [1]. The 3U design of 2019 combined reaction wheels, a star tracker, cold-gas propulsion and an unscented Kalman filter on a microcontroller [2]. Wheels still fail, and a spacecraft that loses them becomes a different spacecraft, as the second history box of this section tells. In the simulator all of these layers fly together, and each is judged against a true attitude that only the scoring can read.

Table 7.1 Signals of the Spacecraft by Role, With Their Reference Values

Symbol	Role	Reference	Range
$\hat{\phi}$, $\hat{\theta}$, $\hat{\psi}$	CVs of pointing, estimated 3-2-1 angles from the orbit frame	0	offsets
e_{cam}	scored CV, true camera from the true line of sight	$\leq 0.1°$	—
$\lvert\Delta\mathbf{h}\rvert$	CV of unloading, excess momentum	0	on 40 %, off 10 %
$\lvert\omega_m\rvert$	CV of detumbling, gyro rate	0.5 °/s SP	0.1–3 °/s
τ_x, τ_y, τ_z	MVs, wheel torques	0	±3 mN m
m_x, m_y, m_z	MVs, coil dipoles	0	$\pm 0.5\,\mathrm{A\,m^2}$
τ_a	DV, drag torque at nadir	2 µN m	0–10
—	DV events, wheel failure, tracker outage, kick, handover	off	events
β_B	DV, magnetometer bias, unmeasured	0	±5 µT
q, ω, $\mathbf{h}$	states	case start	$\lvert h_i\rvert \leq h_{max}$
$\mathbf{b}$	hidden state, gyro bias	7, −9, 5 °/h	walks
ω_m, q_{st}	measured, gyro, star tracker	10 Hz, 1 Hz	blind spells
$\mathbf{B}_m$, $\hat{\mathbf{s}}_m$	measured, magnetometer, sun sensor	10 Hz	none in shadow
$\hat{q}$, $\hat{\mathbf{b}}$	filter states	warm or cold	—

HISTORY Two Wheels and the Pressure of Sunlight (2013 to 2014)

The Kepler space telescope pointed on four reaction wheels until the second of them failed in May 2013, which ended its original mission. Over the next year its teams formulated and tested a new one. Two wheels held the telescope's boresight, and the pressure of sunlight on the solar panels was balanced about the roll axis. Like a pencil balanced on a finger, the balance is unstable, so thrusters fired on a schedule of six hours to keep the roll within bounds, and the momentum that built up on the two wheels was dumped every two days. Roll at the edges of the field grew to two orders of magnitude more than in the original mission, and a rebuilt data pipeline restored much of the photometric precision [17].

7.3 The Spacecraft, Its Orbit and Its Instruments

A rigid 6U of 10 kg carries three reaction wheels on its principal axes, three magnetorquers, a camera with a 2° field of view and four instruments around a circular sun-synchronous orbit at 500 km, as shown in Figure 7.1. Its body axes are x for roll, along the track at nadir, y for pitch, against the orbit normal, and z for yaw, the camera's boresight. Ten states are integrated, the attitude quaternion q of the body against inertial space, the body rate ω in body axes and the momenta $\mathbf{h}$ of the three wheels. Because the engine counts time in minutes, the code multiplies each rate below by 60 s/min. Each signal's role is listed in Table 7.1.

7.3.1 Orbit, Sun and Field

The orbit is circular with radius $R = R_E + 500\,\mathrm{km}$, inclined $i = 97.40°$, and its node turns with the Sun, as shown in Equation (7.1).

$$\begin{aligned} \mathbf{r} &= R\,(\cos u\,\hat{\mathbf{P}} + \sin u\,\hat{\mathbf{Q}}), \qquad u = nt, \qquad n = \sqrt{\mu/R^3} \\ \hat{\mathbf{P}} &= (\cos\Omega,\ \sin\Omega,\ 0), \qquad \Omega = \Omega_0 + \dot{\Omega}t \\ \hat{\mathbf{Q}} &= (-\cos i \sin\Omega,\ \cos i \cos\Omega,\ \sin i) \end{aligned} \tag{7.1}$$

where t is the mission time, $\mu = 3.986\,004\,418 \times 10^{14}\,\mathrm{m^3/s^2}$, $R_E = 6378.137\,\mathrm{km}$, $\dot{\Omega}$ is one turn in 365.2422 days and $\Omega_0 = 157.5°$ puts the ascending node at 22:30 local time with the Sun along the inertial X axis, the March equinox. Then $n = 1.106\,783 \times 10^{-3}\,\mathrm{rad/s}$, the period is 94.62 min, the Sun stands 22.3° from the orbit plane, and a cylindrical shadow of the Earth's radius, without penumbra, covers 34.8 min of every orbit. The orbit frame has $\hat{\mathbf{z}}_O = -\hat{\mathbf{r}}$, $\hat{\mathbf{y}}_O = -\mathbf{r} \times \mathbf{v}/|\mathbf{r} \times \mathbf{v}|$ and $\hat{\mathbf{x}}_O = \hat{\mathbf{y}}_O \times \hat{\mathbf{z}}_O$, and it turns at n about the orbit normal plus the node's slow turn. The Earth turns at $\omega_E = 7.292\,115\,9 \times 10^{-5}\,\mathrm{rad/s}$ with Greenwich on the Sun's line at $t = 0$, and its field is the dipole

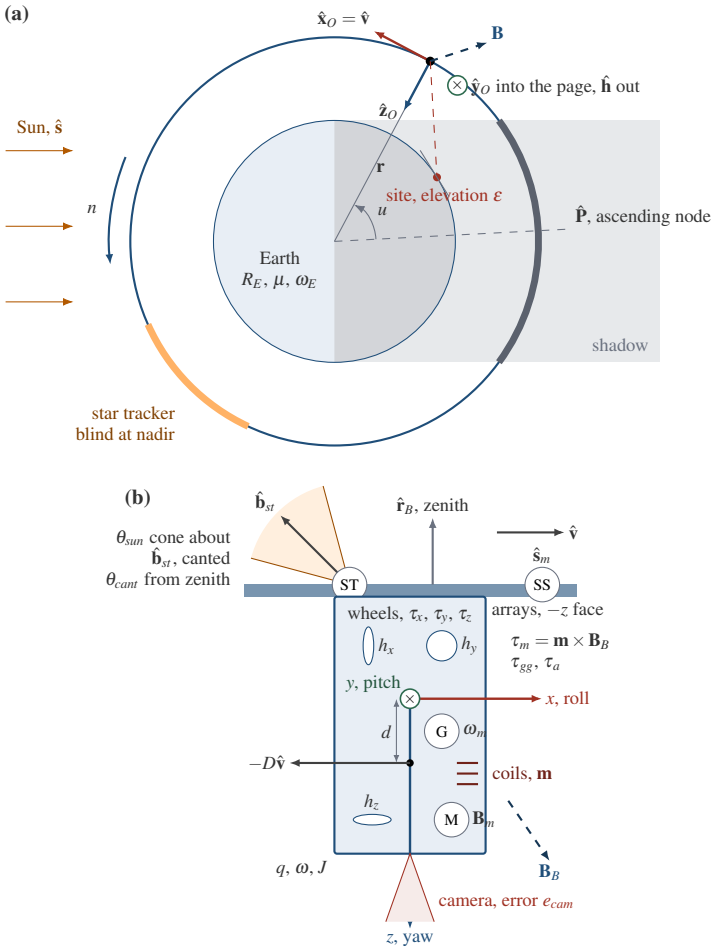


Figure 7.1 The orbit and the spacecraft as modeled, not to scale. (a) The orbit seen from its normal $\hat{\mathbf{h}}$, with the Earth half in night, its shadow away from the Sun $\hat{\mathbf{s}}$, the node $\hat{\mathbf{P}}$, the position $\mathbf{r}$ at argument of latitude u, the orbit frame ($\hat{\mathbf{x}}_O$ along the velocity, $\hat{\mathbf{y}}_O = -\hat{\mathbf{h}}$, $\hat{\mathbf{z}}_O$ to nadir), the field $\mathbf{B}$, a site at elevation ε, and the arcs in shadow (dark) and where the Sun blinds the star tracker at nadir (amber, lighter and labeled). (b) The 6U in the orbit frame, with the wheels' momenta h_i driven by τ_i, the coils $\mathbf{m}$ in the field $\mathbf{B}_B$, the zenith $\hat{\mathbf{r}}_B$, the drag $-D\hat{\mathbf{v}}$ at a center of pressure d from the center of mass along z, the sun sensor (SS) on the arrays, the star tracker (ST) canted θ_{cant} toward the wake inside its Sun cone θ_{sun}, the gyro (G), the magnetometer (M) and the camera with its scored error e_{cam}.

of the thirteenth International Geomagnetic Reference Field for 2020, as shown in Equation (7.2).

$$\mathbf{B} = \left(\frac{a}{r}\right)^3 \left[3(\mathbf{M}\cdot\hat{\mathbf{r}})\hat{\mathbf{r}} - \mathbf{M}\right], \qquad \mathbf{M} = R_Z(\omega_E t)\,(g_1^1,\ h_1^1,\ g_1^0) \tag{7.2}$$

where $g_1^0 = -29\,404.8\,\text{nT}$, $g_1^1 = -1450.9\,\text{nT}$, $h_1^1 = 4652.5\,\text{nT}$ and $a = 6371.2\,\text{km}$ [18], and R_Z turns the Earth-fixed dipole about the spin axis. The dipole is 9.41° off that axis, and along this orbit $|\mathbf{B}|$ runs from 23.69 to 47.37 μT. Two sites fixed to the Earth are the camera's targets, Site A at geocentric 44.36° S, 116.82° W and Site B at 53.15° S, 120.35° W for a handover. A site is in a pass while it sees the satellite above the imaging mask of 5°, and only passes that rise above 20° are tasked,

because lower ones are imaged from more than 60° off nadir. Site A's pass on the fourth orbit lasts 9.10 min and reaches 77.8°.

7.3.2 Body and Wheels

The attitude and the body rate obey Equation (7.3).

$$\begin{aligned} \dot{q} &= \tfrac{1}{2}\, q \otimes \begin{bmatrix} 0 \\ \boldsymbol{\omega} \end{bmatrix}, \qquad \mathbf{v}_I = R(q)\, \mathbf{v}_B \\ J\dot{\boldsymbol{\omega}} &= -\boldsymbol{\omega} \times (J\boldsymbol{\omega} + \mathbf{h}) - \dot{\mathbf{h}} + \boldsymbol{\tau}_{gg} + \boldsymbol{\tau}_a + \mathbf{m} \times \mathbf{B}_B \end{aligned} \tag{7.3}$$

where q is scalar first, $R(q)$ takes body vectors into inertial ones, $J = \mathrm{diag}(0.10, 0.12, 0.05)\,\mathrm{kg\,m^2}$ assigns three moments so that the camera axis has the smallest and pitch the largest, and $\mathbf{B}_B = R(q)^{\mathsf{T}}\mathbf{B}$. The wheels' torque $-\dot{\mathbf{h}}$ is internal, so the inertial total $R(q)(J\boldsymbol{\omega} + \mathbf{h})$ changes only through the external torques. A working wheel delivers its command clipped to τ_{max}, and a torque that would speed it up fades over its last 10 % of speed, as shown in Equation (7.4).

$$\begin{aligned} \dot{h}_i &= \mathrm{sat}(\tau_i,\ \tau_{max}\lambda_i), \qquad \lambda_i = \min\Big(1,\ \frac{h_{max} - |h_i|}{0.1\, h_{max}}\Big) \\ \dot{h}_i &= -c_v\Omega_i - c_c \tanh\Omega_i, \qquad \Omega_i = h_i / I_w \end{aligned} \tag{7.4}$$

where the second line holds for a failed wheel, λ_i applies only when $\tau_i h_i > 0$ and is 1 otherwise, $\tau_{max} = 3\,\mathrm{mN\,m}$ and $h_{max} = 30\,\mathrm{mN\,m\,s}$, so $|h_i|$ never passes h_{max}. At capacity a wheel turns at 625 rad/s, 5968 rpm, on a rotor inertia I_w of $4.8 \times 10^{-5}\,\mathrm{kg\,m^2}$. A working wheel's drive cancels its own bearing friction, so only a failed wheel feels $c_v = 8 \times 10^{-8}\,\mathrm{N\,m\,s/rad}$ and $c_c = 1\,\mu\mathrm{N\,m}$, coasting down and handing its momentum to the body.

7.3.3 Torques From Outside the Spacecraft

Gravity, drag and the coils act on the body, as shown in Equation (7.5).

$$\begin{aligned} \boldsymbol{\tau}_{gg} &= 3n^2\, \hat{\mathbf{r}}_B \times J\hat{\mathbf{r}}_B, \qquad \boldsymbol{\tau}_m = \mathbf{m} \times \mathbf{B}_B \\ \boldsymbol{\tau}_a &= \tau_a\,(\hat{v}_y,\ -\hat{v}_x,\ 0) \end{aligned} \tag{7.5}$$

where $\hat{\mathbf{r}}_B$ and $\hat{\mathbf{v}}$ are the zenith and the velocity direction in body axes. The drag torque is the moment of a drag force $-D\hat{\mathbf{v}}$ applied at a center of pressure displaced d along the camera axis, with $\tau_a = dD = 2\,\mu\mathrm{N\,m}$, so at nadir it is fixed in the body about $-y$, the orbit normal. With a principal axis at nadir the gravity-gradient torque $\boldsymbol{\tau}_{gg}$ vanishes. The position, velocity, field, shadow and orbit frame are evaluated at the start of each 0.1 s step and held through it, while the field turns 0.013° on average.

7.3.4 What the Instruments Report

The instruments alone carry the truth into the flight software. Their noise is drawn inside them once per control step, and the gyro's bias walk, part of the hidden truth, is drawn after each integration step. The gyro and the star tracker report as shown in Equation (7.6).

$$\begin{aligned} \boldsymbol{\omega}_{m,k} &= \frac{\boldsymbol{\varphi}(q_{k-1}^{*} \otimes q_k)}{\Delta t} + \mathbf{b}_k + \frac{\sigma_v}{\sqrt{\Delta t}}\, \boldsymbol{\nu}_k \\ \mathbf{b}_{k+1} &= \mathbf{b}_k + \sigma_u \sqrt{\Delta t}\, \boldsymbol{\nu}'_k \\ q_{st} &= q \otimes \delta q\big(\sigma_{st}(\nu_1 \hat{\mathbf{e}}_1 + \nu_2 \hat{\mathbf{e}}_2) + 6\sigma_{st}\nu_3 \hat{\mathbf{b}}_{st}\big) \end{aligned} \tag{7.6}$$

where $\boldsymbol{\varphi}$ is the rotation vector, so the gyro reports the rotation the body made over its 0.1 s interval Δt, $\sigma_v = 0.05°/\sqrt{\mathrm{h}}$ is its angle random walk, σ_u its bias walk of 0.5 °/h per $\sqrt{\mathrm{h}}$, $\mathbf{b}$ starts at (7, −9,

5) °/h, the ν are standard normal deviates from the case's seeded generator, and $\hat{\mathbf{e}}_1$, $\hat{\mathbf{e}}_2$ span the plane across the tracker's boresight $\hat{\mathbf{b}}_{st}$. The tracker looks out of the zenith face canted $\theta_{cant} = 45^\circ$ toward the wake and reports once a second with $\sigma_{st} = 10$ arcsec across its boresight and six times that about it. It reports nothing while the Sun is within $\theta_{sun} = 30^\circ$ of its boresight outside the shadow, while its boresight is less than $\theta_{limb} = 20^\circ$ above the Earth's limb, the Earth's disc being 68.02° in radius at this height, while the body turns faster than 1 °/s, or during an outage. At nadir the Sun blinds it for 10.85 min of every orbit and the limb never does. The magnetometer reads $\mathbf{B}_B$ every step with 0.1 μT of noise per axis and a bias $(\beta_B, 0, -\beta_B/2)$ when the disturbance sets one, the coils' own field being assumed blanked, and the coarse sun sensor gives the Sun's direction to 1.5° and nothing in the shadow.

7.3.5 The Pass and Its Score

At every step of a tasked pass the score accumulates, from the truth alone, the pass time T_p, the time T_{ok} during which the true camera axis lies within 0.1° of the true line of sight to the site, and the worst such angle. The share imaged is T_{ok}/T_p, and the largest wheel momentum before the pass's first instant is kept apart from the rest of the run.

7.3.6 Epochs, Starting States and Integration

Every case flies the same orbit over the same Earth, starting at its own epoch, the mission time at its $t = 0$. The body starts in the orbit frame or at an offset from it, turning with it, plus any tumble the case adds, with the wheels at zero unless the case loads them. A warm filter starts with an attitude error of (4, −3, 6) μrad and a bias error of (0.04, −0.05, 0.03) °/h under standard deviations of 5 μrad and 0.1 °/h, and a cold one waits for the first tracker reading. A classical Runge-Kutta scheme of fourth order advances the ten states on a fixed 0.1 s step, which is also the period of the flight software, the tracker being read on every tenth step, and every 5 s of flight adds a row to the historian. Each step ends by projecting the quaternion onto unit norm and walking the gyro bias. All random numbers come from one generator seeded at 20261002, as Section 1.6.1 describes for every app. Without the projection Runge-Kutta keeps $|q|$ within 1.9×10^{-10} of one over an orbit of a 10 °/s tumble, and with every external torque off the inertial momentum holds to 6.1×10^{-11} of the 14.2 mN m s in play, 16.0 times closer at half the step. Halving the physics step, with the flight software still at 0.1 s, moves the creep after an orbit by 0.020 % and the worst pointing of case 7 under perfect states by less than 10^{-5}°. All 65 of the application's own checks pass.

7.3.7 Assumptions

A rigid spacecraft with declared inertia. Its principal axes are the body axes and the laws use the declared J, so tripling every moment (yaw's 2.5 times) slows case 5 from 102.3 s to 136.4 s. Flexible arrays, slosh and misaligned wheels would add modes and cross-coupling the model lacks.

Ideal wheels. Inside their torque limit they are torque sources with a linear back-EMF fade, and their motor lag, stiction near zero speed and jitter are absent.

A Keplerian orbit and a dipole field. The orbit ignores the zonal harmonics apart from the node's turn, drag on the orbit and eccentricity, which suits a few orbits, and the Sun is fixed for the five hours of the longest case. The field is the dipole alone, without the terms of degree 2 to 13 that the full reference model carries [18].

One constant drag torque. The drag torque is one declared constant at nadir, turning only with the velocity's direction in the body, while real drag follows the air density. Solar pressure and a residual dipole are not modeled.

Generic instruments. The noise levels stand for no product. The tracker has no latency, stray light or acquisition time, and the orbit and the time are known exactly to the flight software. The filters assume the declared tracker noise, and at 200 arcsec case 7 images 78.0 % of its pass.

Teaching thresholds. The 0.1° requirement, the 80 % wheel limit, the masks, the dead band and the supervisor's thresholds were chosen for teaching and are not a mission specification.

Table 7.2 Model Constants by Class: V for a Show Model Slider, H for a Hidden Parameter and C for a Constant of the Source

Symbol	Meaning	Value	Class
Spacecraft, wheels and coils			
J_x, J_y, J_z	principal moments	0.10, 0.12, 0.05 kg m^2	V
h_{max}, τ_{max}	wheel capacity, torque	30 mN m s, 3 mN m	V
I_w	rotor inertia	4.8×10^{-5} kg m^2	H
c_v, c_c	failed-wheel friction	8×10^{-8} N m s, 1 µN m	V
m_{max}	dipole per coil	0.5 A m^2	V
—	back-EMF fade	last 10 % of speed	C
Instruments			
σ_v	gyro angle random walk	$0.05°/\sqrt{\text{h}}$	V
σ_u	gyro bias walk	0.5 °/h per $\sqrt{\text{h}}$	V
$\mathbf{b}_0$	gyro bias at switch-on	7, −9, 5 °/h	V
σ_{st}	tracker noise across	10 arcsec	V
—	about the boresight	6 σ_{st}	H
θ_{sun}, θ_{limb}, θ_{cant}	tracker exclusions, cant	30, 20, 45°	V
—	tracker rate limit, rate	1 °/s, 1 Hz	H, C
σ_B, σ_{css}	magnetometer, sun sensor	0.1 µT, 1.5°	V
Orbit, field and mission			
$R - R_E$, i, Ω_0	altitude, inclination, node	500 km, 97.40°, 157.5°	C
g_1^0, g_1^1, h_1^1, a	IGRF-13 dipole, 2020	see Eq. (7.2)	C
τ_a	drag torque at nadir	2 µN m	DV
ε_{min}, ε_{task}	imaging mask, tasking	5, 20°	V
—	camera field, requirement	2, 0.1°	V
Δt	step, flight software	0.1 s	C

7.4 What the Inertia and the Field Permit

Whatever controller flies this spacecraft, four properties of Equations (7.2) to (7.5) bound what it can do, and each is checked here on the engine. Their constants are collected in Table 7.2.

7.4.1 A Budget That Fills Every Orbit

The drag torque at nadir is fixed in the body, so one wheel integrates all of it. In one orbit of period T it gains $\tau_a T = 2\,\mu\text{N m} \times 5677\,\text{s} = 11.35\,\text{mN m s}$, 37.85 % of h_{max}, whatever the pointing gains. Only an external torque can return it, and the coils can. A dipole of 0.5 A m^2 in a field of 23.7 to 47.4 µT produces up to 11.8 to 23.7 µN m, six to twelve times the drag, but only across the field. The unloading law of Section 7.5 asks for $|\Delta\mathbf{h}_\perp|/\tau_d$, up to 13.3 µN m at the 40 % excess that switches it on.

🕮 **Pause.** Try Exercise 7.1 before reading on.

7.4.2 The Gravity Gradient Holds the Free Spacecraft

The ordering $J_y > J_x > J_z$ makes nadir pointing stable under the gravity gradient alone. Linearized about the orbit frame, pitch separates from roll and yaw, as shown in Equation (7.7).

$$\begin{aligned} \omega_\theta^2 &= 3n^2\,\frac{J_x - J_z}{J_y} \\ 0 &= s^4 + n^2(1 + 3k_R + k_R k_Y)\,s^2 + 4n^4 k_R k_Y \\ k_R &= (J_y - J_z)/J_x, \qquad k_Y = (J_y - J_x)/J_z \end{aligned} \tag{7.7}$$

where s is the Laplace variable of the coupled roll and yaw motion. With $k_R = 0.7$ and $k_Y = 0.4$ every root is imaginary, and the spacecraft librates at $1.118n$ in pitch and at $0.610n$ and $1.734n$ in roll and yaw, with periods of 84.63, 155.0 and 54.6 min. The engine agrees. Left in manual with no drag and a 2° pitch offset, a start that no case offers, the spacecraft librates in pitch with a period of 84.65 min for four orbits while roll and yaw stay within 0.05°, and from a 2° roll offset roll and yaw

exchange through the faster coupled mode, with zero crossings every 54.63 min, yaw reaching 2.79°. The restoring torque in pitch is $3n^2(J_x - J_z) = 3.2\,\text{nN m}$ per degree, about 1/600 of the drag, so the ordering matters to a spacecraft left alone and very little to one under control.

7.4.3 The Field Against the Stored Momentum

Two frames meet in magnetic unloading. With the body held on nadir the wheels' momentum is fixed in inertial space, apart from what external torques add. In case 4 with unloading off and the drag torque at zero, the excess keeps its inertial direction within 0.03° over two orbits (0.01 to 0.05° on five other seeds), while the roll wheel's 15 mN m s moves to the yaw wheel a quarter of an orbit later as the body turns under it. The field lies close to the orbit plane, on average 1.6 to 9.1° out of it in the first four orbits, radial over the magnetic poles and along the track over the magnetic equator. It therefore makes one turn an orbit in the orbit frame and two in inertial space, and so two against the stored momentum. With $\Delta\mathbf{H} = R(q)\,\Delta\mathbf{h}$ the excess in inertial axes and $\hat{\mathbf{b}}$ the field's direction, the law's torque $-k\Delta\mathbf{h}_\perp$ and its orbit average are given by Equation (7.8).

$$\frac{\mathrm{d}\Delta\mathbf{H}}{\mathrm{d}t} = -k\,(I - \hat{\mathbf{b}}\hat{\mathbf{b}}^\mathsf{T})\,\Delta\mathbf{H} \;\approx\; -k\,\langle I - \hat{\mathbf{b}}\hat{\mathbf{b}}^\mathsf{T}\rangle\,\Delta\mathbf{H} \tag{7.8}$$

where $k = 1/\tau_d$ and the angle brackets average over the orbit, the form of analysis applied to an inertially fixed spacecraft in [5]. Over the first three orbits $\langle\hat{\mathbf{b}}\hat{\mathbf{b}}^\mathsf{T}\rangle$ in the axes $(\hat{\mathbf{P}}, \hat{\mathbf{Q}}, \hat{\mathbf{h}})$ is diag(0.493, 0.491, 0.016), with no off-diagonal term above 0.004. An excess along the orbit normal therefore decays with a time constant of 15.24 min, close to $\tau_d = 15\,\text{min}$, and an excess in the plane with 29.5 to 29.6 min, twice as long. The engine follows, in runs started from a state that no case offers. With 30 % on one wheel, the coils on with the dead band open and no drag, the pitch excess falls to a tenth in 36.2 min against a predicted 35.1, the roll excess, along $\hat{\mathbf{Q}}$ at the start, in 64.4 min against 67.9, and the yaw excess, along $-\hat{\mathbf{P}}$, in 70.3 min against 68.1, as shown in Figure 7.2(a). The excess in the plane falls in steps, quickly while the field lies across it and hardly at all while the field passes along it, four times an orbit. The drag's excess builds up along the orbit normal, the direction the law reaches most easily.

7.4.4 B-dot and the Rate Along the Field

For a spin fast against the field's turning, $\dot{\mathbf{B}}_B \approx -\boldsymbol{\omega} \times \mathbf{B}_B$, and the B-dot law of Section 7.5 gives the torque of Equation (7.9).

$$\mathbf{m} = -\frac{k_B}{|\mathbf{B}_B|^2}\,\dot{\mathbf{B}}_B \quad\Rightarrow\quad \tau_m = \mathbf{m} \times \mathbf{B}_B \approx -k_B\,\omega_\perp \tag{7.9}$$

where $\omega_\perp$ is the part of the rate across the field. The law removes that part and cannot touch the rate along the field. A strong gain removes it quickly and leaves the body turning about the field line, which then has to wait for the field to turn. Figure 7.2(b) shows the price, with each gain set before the run. Case 2's tumble falls under 0.5 °/s fastest at 0.4 and 0.5 mN m s, in 26.655 and 26.81 min, against 48.285 and 46.19 min at 0.20 and 0.25 mN m s, the settings either side of the 0.22 mN m s that the application's guide evaluates from the criterion of [7], 69.67 min at 2 and 85.1 to 86.1 min from 6 to 20. Above 0.5 mN m s the coils spend longer at their limit, 8.2 min at 0.5, 25.0 at 2 and 69.8 at 8, so a larger gain buys no more torque, only more alignment.

🕮 **Pause.** Try Exercise 7.2 before reading on.

7.5 The Flight Software as Written

The flight software works through four stages on each 0.1 s step, the instruments, the filters, the supervisor and the laws. Apart from a teaching switch, Perfect, that hands the laws the true attitude and rates, no stage of it sees the truth. The velocity-form PID of Section 1.6.2, which most apps share, has no role here. No law integrates an error, so nothing can wind up against a wheel's limit and no anti-windup is needed. Table 7.3 holds the settings, their defaults and their ranges.

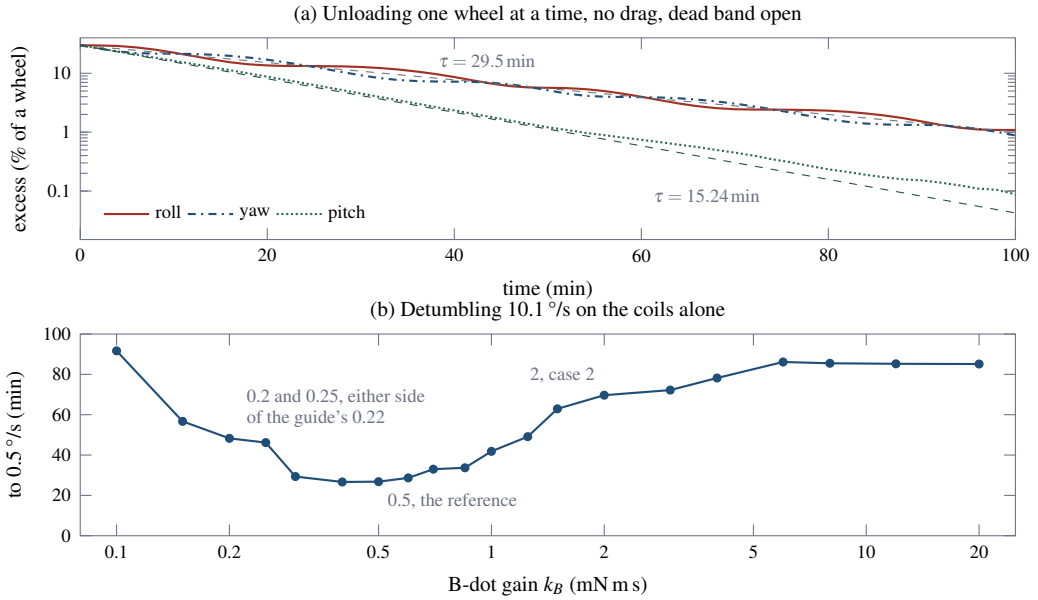


Figure 7.2 What the field allows, measured on the engine. (a) Excess momentum after 30 % is placed on one wheel, with the coils on, no dead band and no drag (roll solid, yaw dash-dotted, pitch dotted), against the orbit-averaged decays of Equation (7.8) (thin dashed). (b) Time for B-dot to bring case 2's 10.1 °/s tumble under 0.5 °/s, against the gain set before the run.

Table 7.3 Flight Software Settings, With Their Defaults and Ranges

Symbol	Setting	Default	Range
—	mode	Auto	one mode
—	attitude estimate	EKF + bias	perfect, no bias
K_p, K_d	attitude and rate gains	0.0625 s^{-2}, 0.45 s^{-1}	to 0.5, 2
ω_{lim}	slew rate limit	1 °/s	0.1–6
—	pointing law	eigenaxis	three axes, MPC
—	MPC preview of the site's path	on	off
—	roll, pitch, yaw offsets	0	±180, ±89, ±180
—	momentum unloading	on	off
τ_d	unloading time constant, $1/k$	15 min	2–120
—	dead band, on and off	40 %, 10 %	1–90, 0–80
$h_{y,SP}$	pitch wheel momentum target	0	±60 %
k_B	B-dot gain	0.5 mN m s	0.05–20
—	detumbled below, for 60 s	0.5 °/s	0.1–3
—	lead before a pass	2 min	0.5–6
$\hat{\sigma}_v$, $\hat{\sigma}_u$	filter's gyro noise, bias walk	as the gyro	to 1, 10
$\hat{\sigma}_{b0}$	filter's bias allowance at start	20 °/h	0.1–100

7.5.1 Two Filters on One Gyro

Two multiplicative filters work in parallel on the same readings, one that estimates the gyro bias as a state, as Section 1.4.6 describes, and one that does not, and the setting selects which one the laws use.

The filter with the bias propagates and updates as shown in Equation (7.10).

$$
\begin{aligned}
&\hat{q} \leftarrow \hat{q} \otimes \delta q\big((\omega_m - \hat{\mathbf{b}})\Delta t\big), \qquad P \leftarrow \Phi P \Phi^{\mathsf{T}} + Q \\
&\Phi = \begin{bmatrix} I - [\hat{\omega}\times]\Delta t + \frac{1}{2}[\hat{\omega}\times]^2\Delta t^2 & -I\Delta t \\ 0 & I \end{bmatrix} \\
&Q = \begin{bmatrix} (\sigma_v^2\Delta t + \sigma_u^2\Delta t^3/3)\, I & -\frac{1}{2}\sigma_u^2\Delta t^2\, I \\ -\frac{1}{2}\sigma_u^2\Delta t^2\, I & \sigma_u^2\Delta t\, I \end{bmatrix} \\
&\mathbf{z} = 2\,\mathrm{sgn}(w)\,\mathrm{vec}(\hat{q}^* \otimes q_{st}) \\
&K = PH^{\mathsf{T}}(HPH^{\mathsf{T}} + R_{st})^{-1}, \qquad \begin{bmatrix} \delta\theta \\ \delta\mathbf{b} \end{bmatrix} = K\mathbf{z} \\
&\hat{q} \leftarrow \hat{q} \otimes \delta q(\delta\theta), \qquad \hat{\mathbf{b}} \leftarrow \hat{\mathbf{b}} + \delta\mathbf{b}
\end{aligned}
\tag{7.10}
$$

where $\hat{\omega} = \omega_m - \hat{\mathbf{b}}$, w is the scalar part of $\hat{q}^* \otimes q_{st}$, $H = [I\ 0]$, the covariance is updated in the Joseph form $P \leftarrow (I - KH)P(I - KH)^{\mathsf{T}} + KR_{st}K^{\mathsf{T}}$, and $R_{st} = \sigma_{st}^2(I - \hat{\mathbf{b}}_{st}\hat{\mathbf{b}}_{st}^{\mathsf{T}}) + (6\sigma_{st})^2\hat{\mathbf{b}}_{st}\hat{\mathbf{b}}_{st}^{\mathsf{T}}$ matches the declared tracker. The filter assumes the gyro's own σ_v and σ_u. A cold filter starts at the first tracker reading with $\hat{q} = q_{st}$, $\hat{\mathbf{b}} = 0$, an attitude variance of σ_{st}^2 and a bias allowance of 20 °/h. The other filter drops the bias rows and treats the gyro as unbiased, so whenever the tracker is blind it integrates the bias into the attitude. The laws use $\hat{q}$ and the rate $\omega_m - \hat{\mathbf{b}}$. A bias state serves the same purpose in the vessel observer of Chapter 6, where it absorbs the wind and the current.

7.5.2 Supervisor and Modes

In Auto the supervisor moves through four modes. Detumble runs B-dot with the wheels idle until the gyro has read under 0.5 °/s for 60 s. Safe turns the arrays onto the measured Sun until the filter is running with its own standard deviation under 0.05° and the Sun is within 10° of the arrays for 30 s. Nadir flies the orbit frame turned by the three offsets, and target tracking points the camera at the tasked site from 2 min before a tasked pass rises above the mask until 30 s after it sets. The target reference puts z on the line of sight with x as near the velocity as the line of sight allows, and its rate and acceleration come from central differences of that frame with a step of 1 s. Without a running filter the pointing modes fall back to safe.

7.5.3 Pointing About the Eigenaxis

The pointing law closes the error of the estimate against the reference through a rate command and an inner rate loop, as shown in Equation (7.11).

$$
\begin{aligned}
&q_e = q_r^* \otimes \hat{q}, \qquad \phi = \varphi(q_e) \\
&\omega_c = -\mathrm{sat}_{\|\cdot\|}\Big(\frac{K_p}{K_d}\phi,\ \omega_{lim}\Big) \\
&\mathbf{u} = J\big[K_d(\omega_r + \omega_c - \hat{\omega}) + \alpha_r\big] + \hat{\omega} \times (J\hat{\omega} + \mathbf{h}) \\
&\tau_i = \mathrm{sat}\big((\mathbf{m} \times \mathbf{B}_m - \mathbf{u})_i,\ \tau_{max}\big)
\end{aligned}
\tag{7.11}
$$

where q_r is the reference, ϕ the rotation vector of the error taken the short way, $\mathrm{sat}_{\|\cdot\|}$ limits the length of the vector and not its parts, as Section 1.4.2 explains, and ω_r and α_r are the reference's rate and acceleration in body axes. Unsaturated, $\mathbf{u}$ is the quaternion feedback $-JK_p\phi - JK_d(\hat{\omega} - \omega_r) + J\alpha_r$ with the gyroscopic term cancelled, and the defaults give $\omega_n = 0.25\,\mathrm{rad/s}$ with $\zeta = 0.9$. Limiting the length keeps a slew on the eigenaxis. The three-axis alternative limits each 3-2-1 angle of q_e in its own loop, as three single-axis controllers would. The wheels deliver $\mathbf{u}$ and also take up the torque the coils are believed to apply, computed from the measured field. A positive error about any axis is driven back by a negative torque about it, as the application's direction checks confirm. In the

convention of Section 1.3 the pointing loop is therefore reverse acting on the body torque $\mathbf{u}$ and direct acting on the wheel torques, whose positive sense, as the application labels it, spins the body the other way. Safe mode uses the same gains on the sun sensor and the raw gyro, with ω_c turning $-z$ onto the measured Sun and $\omega_c = 0$ in the shadow, a rate hold that drifts with the bias.

7.5.4 The Coils

The coils serve three laws, as shown in Equation (7.12).

$$\begin{aligned}
\dot{\mathbf{B}}_{f,k} &= \gamma \dot{\mathbf{B}}_{f,k-1} + (1-\gamma)\,\frac{\mathbf{B}_{m,k} - \mathbf{B}_{m,k-1}}{\Delta t} \\
\mathbf{m}_B &= -\frac{k_B}{|\mathbf{B}_m|^2}\,\dot{\mathbf{B}}_f \\
\mathbf{m}_U &= \frac{k}{|\mathbf{B}_m|^2}\,(\Delta\mathbf{h} \times \mathbf{B}_m) \\
\mathbf{m}_F &= u_j\,\frac{\mathbf{B}_m \times \hat{\mathbf{e}}_j}{|\mathbf{B}_m \times \hat{\mathbf{e}}_j|^2}
\end{aligned} \tag{7.12}$$

where $\gamma = \mathrm{e}^{-\Delta t/\tau_f}$ with $\tau_f = 1\,\mathrm{s}$ filters the field's rate for B-dot ($\mathbf{m}_B$), $\Delta\mathbf{h} = \mathbf{h} - (0, h_{y,SP}, 0)$ from the wheels' tachometers is the excess the unloading law ($\mathbf{m}_U$) acts on, with its torque $-k\Delta\mathbf{h}_\perp$, and $\mathbf{m}_F$ is the least dipole that gives the torque u_j about the axis $\hat{\mathbf{e}}_j$ of a failed wheel, the directional actuator of Section 1.4.7. Unloading switches on above an excess of 40 % of one wheel and off below 10 %, and it is suspended while the coils stand in for a wheel. Every dipole is scaled along its own direction so that no coil passes $0.5\,\mathrm{A\,m^2}$. The order of the cross product matters. Written as $\mathbf{B} \times \Delta\mathbf{h}$, as the application's first design had it, the law with $\tau_m = \mathbf{m} \times \mathbf{B}$ gives $+k\Delta\mathbf{h}_\perp$ and fills the wheels. The code uses the order that empties them, which the application's checks confirm by showing that the torque opposes the excess and never has a part along $\mathbf{B}$.

7.5.5 A Predictive Pointing Law

The pointing law's third value, MPC, replaces $\mathbf{u}$ of Equation (7.11) in nadir and target tracking by the first move of a plan re-solved at every decision, the receding-horizon form of Section 1.6.3, whose stability and optimality are reviewed in [19], applied to spacecraft attitude in explicit form in [20] and surveyed for aerospace systems in [21]. The wheels, or two wheels and $\mathbf{m}_F$ after a failure, deliver its $\mathbf{u}$ through the last line of Equation (7.11), and detumble, safe mode, unloading and manual mode are unchanged. Its model is Equation (7.3) at the declared inertia $J_0 = \mathrm{diag}(0.10, 0.12, 0.05)\,\mathrm{kg\,m^2}$, frozen when the application loads, written about the supervisor's reference at each decision as shown in Equation (7.13).

$$\begin{aligned}
\dot{\phi} &= \delta\omega, \qquad \delta\omega = \hat{\omega} - \omega_r, \qquad \dot{\mathbf{h}} = \tau_m - \mathbf{u} \\
\delta\dot{\omega} &= J_0^{-1}(\mathbf{u} - \mathbf{g}) + \hat{\mathbf{d}} - \alpha_r, \qquad \mathbf{g} = \hat{\omega} \times (J_0\hat{\omega} + \mathbf{h})
\end{aligned} \tag{7.13}$$

where ϕ, ω_r and α_r are those of Equation (7.11), $\mathbf{h}$ comes from the tachometers, $\tau_m = \mathbf{m} \times \mathbf{B}_m$ and the gyroscopic torque $\mathbf{g}$ are held over the horizon, and $\hat{\mathbf{d}}$ is an estimated disturbance acceleration. The term $\phi \times \delta\omega$ is dropped, which is exact along a fixed eigenaxis. With wheel j failed, u_j comes from the coils, the other wheels take $\dot{h}_i = -u_i - a_i u_j$ with $a_i = B_{m,i}B_{m,j}/|\mathbf{B}_m \times \hat{\mathbf{e}}_j|^2$, and h_j leaves the model. It comes from the physics and not from a fit, since stepping the torque could reveal only $1/J_0$, 0.573, 0.477 and $1.146\,^\circ/\mathrm{s^2}$ per mN m about roll, pitch and yaw. Two checks confirm it. With no bound or band active the first move equals the discrete LQR's on the same weights to 10^{-6}, and a fresh controller handed only what each decision received reproduces 599 of 599 moves bit for bit on a spacecraft with $J_x = 0.2\,\mathrm{kg\,m^2}$, drag and magnetometer bias.

Estimator. On each axis a two-state Kalman filter with a constant gain, solved once from the Riccati equation, runs on $[\omega_i, d_i]$ at the 0.1 s step, driven by the torque applied and measuring $\hat{\omega}_i$, with

process variances $(2\times10^{-6}\,\mathrm{rad/s})^2$ and $(2\times10^{-8}\,\mathrm{rad/s^2})^2$ a step and the gyro's $\sigma_v^2/\Delta t$. Integrating disturbances of this kind make a predictive controller offset-free [22], and after 10 min of case 3 the pitch estimate stands at −1.986 µN m against the 2 µN m of drag. A jump of more than 1 °/s in one step while every wheel is under $0.9h_{max}$ is read as a kick, which resets the rate and leaves $\hat{\mathbf{d}}$ alone. The filter runs under every law, so a switch starts converged. Because the gyro averages over its last step, the plan's starting rate is advanced half a step with the acceleration the applied torque and $\hat{\mathbf{d}}$ give, 0.17 °/s on yaw at 3 mN m.

The plan. Every 0.5 s on an integer step clock, and at once whenever the relative rate leaves the plan's own prediction by more than 0.02 °/s, the controller solves Equation (7.14) over $N = 120$ steps of $T_p = 0.5$ s, 60 s in all, with the input held in ten move blocks (lengths 1, 1, 2, 3, 5, 8, 12, 18, 30 and 40), and applies the first.

$$\begin{aligned}\min\ &\sum_{k=1}^{N}\left(Q_\phi|\phi_k|^2+Q_\omega|\delta\omega_k|^2\right)+\|\phi_N\|_{P_\phi}^2+\|\delta\omega_N\|_{P_\omega}^2\\&+S\sum_b|\Delta\mathbf{u}_b|^2+R\sum_{k=0}^{N-1}|\mathbf{u}_k-\mathbf{u}_0^h|^2\\&+\sum_\ell\left(\rho_\ell s_\ell^2+\sigma_\ell s_\ell\right)\\\text{s.t. }&|\tau_{m,i}-u_{k,i}|\le\tau_{max},\quad |h_{k,i}|\le0.9\,h_{max}+s_{h,i}\\&|\delta\omega_{k,i}|\le\omega_{lim}\max(|\hat{e}_i|,0.1)+s_{k,i}\end{aligned}\tag{7.14}$$

in degrees, °/s, mN m and mN m s, where $Q_\phi = 3$, $Q_\omega = 0.1$ and $S = R = 0.01$, $\|\mathbf{x}\|_P^2 = \mathbf{x}^\mathsf{T}P\mathbf{x}$, P_ϕ and P_ω are the diagonal of the discrete LQR's Riccati solution for each axis, $\Delta\mathbf{u}_b$ is the change at each block boundary from the move in force, $\mathbf{u}_0^h = \mathbf{g} - J_0\hat{\mathbf{d}}$ is the torque that holds the reference, and $\hat{\mathbf{e}}$ is the present error's eigenaxis. The torque bound is hard, as the allocation clamps it, and with a wheel failed the coils' authority about its axis on the measured field bounds u_j. The rate box, whose corner lies at ω_{lim} along $\hat{\mathbf{e}}$ so that no direction exceeds $1.01\omega_{lim}$, is soft with a slack at every judged step and $\rho = \sigma = 10^6$. The wheels' ceiling at the start of the motor's fade is soft with one slack, $\rho = 10^5$ and $\sigma = 10^4$, and is not judged on a wheel where the momentum needed to hold the reference alone comes within 1 % of capacity of it, because only the coils can remove that momentum. Bands are judged at block ends, where a held torque puts their extremes, and no move cap is needed, because the wheels have no torque-rate limit. While every wheel works the problem separates exactly into three 3-state, 10-variable quadratic programs given the coupled problem's ridge of 0.028, whose moves equal the coupled solution's bit for bit on 1,579 recorded decisions, and a failed wheel couples the axes through the coils, so the coupled program is solved. A plan is accepted only with an optimal status, finite moves, predictions, cost and slacks, every planned torque inside its box and the right shapes. Otherwise the eigenaxis law, computed at every step, takes the torque at once, the historian is marked, and control returns to the plan, blended over 1 s, with the next accepted solution. The preview, which may be switched off, is the tasked site's look-frame acceleration over the horizon from the orbit the flight software knows.

Tuning and cost. The weights were chosen by a rule fixed before any grid: the most of case 10's pass within 0.1°, with the true relative rate under $1.02\omega_{lim}$ on cases 5, 7 and 10, no fallback, case 7 whole and case 5 settled no later than the eigenaxis law. Its first winner, $Q_\omega = 0.3$, imaged 5.0 % of the pass with J_x at its slider's low end of 0.02 kg m^2, because a torque planned for J_0 acts up to six times harder than planned for the 0.5 s it is held. The re-plan on a broken prediction was then added and the rule amended, openly, to require 90 % imaged and under 1 s above $1.05\omega_{lim}$ with each moment at 0.02 kg m^2 and with all at 0.3 kg m^2. Of 36 sets 33 meet it, and the winner above images 94.26 % against the first winner's 94.24 %. A decision costs about 0.6 ms in Chrome's own frame loop on a loaded host, up to 1.3 ms at low speed. The speeds run from 0.25 to 60 simulated minutes per second, so the default of 1 min/s, 60 times real time, asks for 120 decisions a wall second, which

Table 7.4 The Ten Cases and the Graded Challenge

#	Change from the reference line	Teaching point
1	manual, 1 mN m on the roll wheel from 0.5 min	a wheel moves momentum
2	detumble from 5.8, −5.8, 5.8 °/s, $k_B = 2$ mN m s	a strong gain is slow
3	nadir, unloading off, three orbits	the wheels fill
4	nadir, wheels at 50, −60, 0 %	across a turning field
5	slew at 0.5 min to roll 70, pitch 60, yaw 90°	eigenaxis or three axes
6	nadir, no-bias filter, filters cold, 14 min before the Sun's window	coasting on the gyro
7	Site A's pass, 8 min after the start	a half-blind tracker
8	as 7, roll wheel fails at 12.5 min	honest infeasibility
9	safe mode from 30, −40, 20° offsets, through the shadow	power on two sensors
10	as 7, handover to Site B at 12 min, MPC	a slew planned in its limits
C	three orbits then the pass, unloading off, no-bias filter	graded challenge

took 7.5 to 15 % of a core in two measurements, past the tenth of a core allowed to every app at 1×, where real time costs 0.15 %. A frame guard stops stepping after 25 ms, so a request for 20 or 60 min/s runs at 11 to 13 min/s and 32 to 37 frames a second, against 15.2 and 16.2 min/s at 15.3 and 5.5 frames without it. With a wheel failed the coupled program costs 2.0 to 2.2 ms, 27 % of a core at 1 min/s, and runs at 3.4 min/s at the top speeds.

7.5.6 Hand Control, and What Each Model Knows

Under hand control the operator sets the three wheel torques and the three dipoles directly, and in Auto the manual settings follow the commands after every control step, rounded to the 0.01 mN m and 0.01 A m^2 that the sliders display, so a switch to manual starts from the last commands. Three models are kept apart. Equations (7.1) to (7.6) simulate the spacecraft. The flight software carries a lighter one, the rigid body with the declared J, an exact orbit, Earth rotation and site geometry, the filters' gyro model and the field it measures, with nothing of the drag or of the gravity gradient. Its predictive law reduces that model to the linear error dynamics of Equation (7.13), which of the run's parameters reads only the actuator limits that the allocation also reads. Equations (7.7) to (7.9) serve the analysis, to interpret the runs, and nothing is identified from data.

7.6 Ten Cases and a Five-Hour Challenge, Measured

Each case takes the defaults of Table 7.3 as its starting line, Auto with the bias filter, the eigenaxis law, unloading on and 2 µN m of drag, and alters only the items its own row of Table 7.4 lists. All of the results in this section come from the engine alone, stepped as the browser steps it, at the default seed. Each shipped scenario gives identical logs whichever way it is reached, and Reset and reload behave as Section 1.6.4 describes. Apart from case 1's kick and switch to Auto, each variant below makes its change before the run, which gives the same run as the change carried through a restart. Where the instruments' noise matters, the text gives the range over five other seeds. The results are collected in Table 7.5.

7.6.1 A Wheel Moves Momentum

Case 1 starts at nadir in manual with the wheels still, and at 0.5 min a script puts 1 mN m on the roll wheel and takes it away 10 s later. The pulse leaves the wheel with 10.0 mN m s, 33.3 % of its capacity, and the body rolling the other way at 5.73 °/s, still 5.74 °/s at 10 min. The total angular momentum starts at 0.13 mN m s, the spacecraft's share of the orbit's own rotation, $J_y n$, reaches 0.19 by the pulse as the drag pushes on a body nothing holds, and is 0.22 after it and 0.19 at 10 min. In a restarted run a deployment kick at 1 min is external and lifts the total to 3.91 mN m s. Switched to Auto at 3 min, the pointing law has the camera within 0.1° of nadir at 5.995 min, and the wheels then hold 3.90 mN m s between them at 12 min, the kick's momentum stored and not removed. Nothing in manual depends on the instruments' noise, so every seed gives these values.

Table 7.5 Each Case's Measured Result, Default Seed

Case and configuration	Result
1, as shipped	pulse 10.0 s, wheel 10.0 mN m s, body −5.73 °/s, total 0.13, 0.19, 0.22 mN m s
1, kick at 1, Auto at 3 min	total 3.91 mN m s, within 0.1° at 5.995 min, wheels hold 3.90 mN m s
2, $k_B = 2$	1 °/s at 34.5 min, 0.5 °/s at 69.7 min, safe at 70.8, nadir at 80.6 min
2, $k_B = 0.5$ and 8	0.5 °/s at 26.8 and 85.5 min
3	37.84 % and 75.69 % after one and two orbits, 98 % at 245.0 min, 1° off at 250.8 min
4	78.1 % to 10 % by 58.6 min, along **B** up to 84 % of it, on again at 139.1 min
4, unloading off	97.75 % at 60 min
5, eigenaxis	90.62° flown for 90.45°, 102.3 s, 0.94 °/s, 0.85 mN m
5, three axes	105.28° flown, 86.4 s, 1.69 °/s, axis wanders 25.3°
5, eigenaxis at 6 °/s	5.10 mN m asked, 1.7 s at the limit, 30.9 s
6, no bias	blind 11.55 min, worst 2.35°, 0.046° a minute after
6, bias	blind 10.84 min, worst 0.054°, bias within 1 °/h at 0.60 min
7, bias, no bias, perfect	100 %, 51.15 %, 100 % within 0.1°, worst 0.026, 0.905, 0.015°
8	81.97 %, field within 3.46° of roll at 16.82 min, worst 5.82°
8, four other settings	81.56 to 84.75 %
9	within 5° at 1.02 min, 8.65° at sunrise, 6.28° with no drag
10, MPC, eigenaxis	on Site B in 39.6 and 52.1 s, 94.26 % and 92.44 % imaged

7.6.2 A Tumble Against the Field

Case 2 releases the spacecraft at 10.1 °/s with B-dot at 2 mN m s. The rate halves in 5.7 min and is 2.51 °/s at 12 min, with the coils on their limit for 25.0 min, but the last degree per second is slow, 1 °/s at 34.5 min and 0.5 °/s only at 69.7 min. Between 30 and 60 min the cosine of the angle between the rate and the field averages 0.984, so the spacecraft is turning almost exactly about the field line, where Equation (7.9) gives it no torque. The supervisor hands over to safe mode at 70.8 min, between 70.9 and 71.2 min on five other seeds, and to nadir at 80.6 min, once the filter, started cold at its first tracker reading, is under 0.05° with the arrays on the Sun.

7.6.3 The Wheels Fill

Case 3 holds nadir for three orbits with unloading off. The camera stays within 0.018° of nadir on average, 0.076° at worst, while the pitch wheel gains 37.84 % after one orbit and 75.69 % after two, within 0.01 % of $\tau_a T / h_{max}$ and its double. At 245.0 min, 2.59 orbits in, the wheel passes 98 % of its capacity and the fading motor can absorb no more. The drag then turns the body, the camera is 1° off nadir at 250.8 min, and the body then turns freely, 136.5° off at the end of the third orbit and anywhere from 17.9 to 143.5° on five other seeds. No pointing gain changes this, because the momentum has to leave the spacecraft.

> **TRY IT IN THE APP** **3 · Nadir Hold: The Wheels Creep**
>
> Load the case, choose 20 min/s and press Run. Open the Momentum view and watch the pitch wheel's bar grow while the camera stays on nadir. The chapter reports 37.84 % of capacity after one orbit and 75.69 % after two. Past 98 %, at 245.0 min, the wheel can absorb no more and the camera leaves nadir.

7.6.4 Unloading Across a Turning Field

Case 4 starts with the roll wheel at 50 % and the pitch wheel at −60 %, an excess of 78.1 % of one wheel with 32.5 % of a wheel along the field. The coils sit at their limit for the first 7.4 min, and the law brings the excess under 10 % in 58.6 min. While the law runs, the share of the excess that lies along the field swings from a peak to almost nothing in 8 to 19 min, its peaks come 22 to 26 min apart, and it reaches 84 %. The part along the field is 27.8 % of a wheel at 22 min, as shown in Figure 7.3, and the excess falls fastest when the field has turned across it. After the first descent the drag refills the pitch wheel by about 38 % an orbit and the dead band cycles, on again at 139.1 min and off at 172.9 min, with the excess never above the 40.0 % that switches the law on. With unloading off the same start reaches 97.75 % at 60 min. The seed moves none of these times by more than 0.1 min.

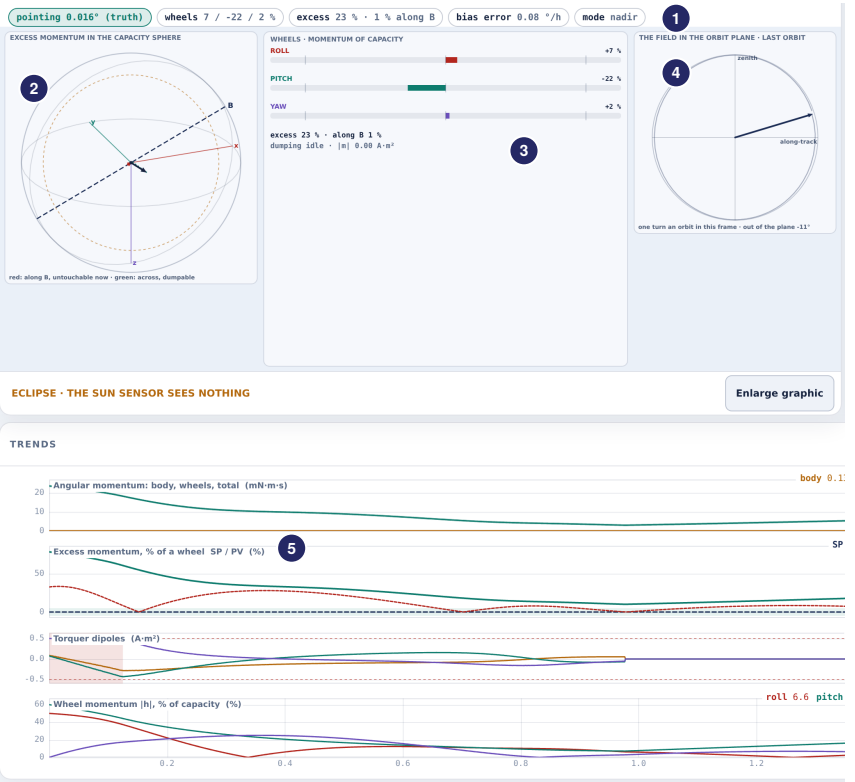


Figure 7.3 The spacecraft in case 4, Momentum dumping, at $t = 94.62$ min, one orbit (the clock reads 1.58 h), with no control changed, in the Momentum view with the 1.58 h trend window, cropped to the plant view and the trends: (1) the badges, (2) the capacity sphere, (3) the wheels' bars, (4) the field panel and (5) the excess strip. The badges read the camera 0.016° off its reference (truth), the wheels at 7, −22 and 2 %, an excess of 23 % with 1 % along **B**, a bias error of 0.08 °/h and nadir mode, and the status line reads Eclipse, the sun sensor sees nothing. The capacity sphere holds the small excess, almost all across the dashed field line, with the law idle in its dead band, and the field panel traces one turn of the field in the orbit plane over the last orbit, the field now −11° out of the plane. The strips, cut short of the orbit's end, show the excess falling from 78.1 % to 10 % by 58.6 min, its part along **B** (dashed) peaking at 27.8 % of a wheel at 22 min, the dipoles at their limit (shaded) for 7.4 min and idle after the law switches off, and the roll wheel's momentum passing to the yaw wheel, 0.01 % and 25.0 % near 21 min, as the body turns under the stored momentum.

7.6.5 One Axis or Three

Case 5 commands roll 70°, pitch 60° and yaw 90° from the orbit frame at 0.5 min, which compose a single rotation of 90.45° about one axis. The eigenaxis law turns the body through 90.62°, 90.48° with perfect states, at up to 0.94 °/s with its error axis within 0.3° of where it started and a peak wheel torque of 0.85 mN m, and the camera settles within 0.1° of its reference 102.3 s after the command. The three-axis law settles sooner, at 86.4 s, but turns the body through 105.28°, 16 % more, at up to 1.69 °/s and with an axis that wanders 25.3°, because three loops each held to 1 °/s add up to nearly $\sqrt{3}$ times the limit in a direction that is not the eigenaxis. At a limit of 6 °/s the eigenaxis slew asks one wheel for 5.10 mN m against its 3, spends 1.7 s at the torque limit and settles in 30.9 s with its axis bent by only 1.0°. On five other seeds the settling times move by at most 0.5 s.

🕮 **Pause.** Try Exercise 7.3 before reading on.

7.6.6 Coasting Through the Blind Window

Case 6 holds nadir with both filters starting cold, 14 min before the Sun enters the tracker's cone. The bias filter, started at the first tracker reading 1 s in, has the bias within 1 °/h at 0.60 min and within 0.3 °/h at 1.37 min, and through a window of 10.84 min it holds the camera within 0.054°, its bias estimate 0.18 °/h off as the window opens and 0.35 °/h as it closes. The filter that leaves the bias out integrates the gyro as it reads, about 11.4 °/h across the camera axis, and the pointing loop holds that drifting estimate on nadir. The camera reaches 2.35° off, more than its whole field, and the window lasts 11.55 min because the drifting attitude keeps the Sun in the cone. A minute after the tracker returns the camera is back within 0.046°. Perfect states hold 0.015°. The noise moves these results more than any other case's. On five other seeds the worst angle in the window is 2.32 to 2.46° without the bias state and 0.036 to 0.102° with it, and the bias estimate comes within 0.3 °/h anywhere from 0.65 to 4.19 min after the start.

> **TRY IT IN THE APP** **6 · The Gyro Bias and the Blind Window**
>
> Load the case and press Run. The shipped filter leaves the gyro bias out: watch the pointing badge while the Sun blinds the star tracker, and the camera drifts to 2.35° off nadir. Then press Reset, set the Attitude estimate to EKF + bias on the MODE card before the window opens at about 14 min, and run again. The worst angle in the window falls to 0.054°.

7.6.7 A Pass With the Tracker Half Blind

Case 7 enters target tracking 2 min before Site A rises and reaches the moving reference 80.7 s later. Through the 9.10 min pass the body turns at up to 0.86 °/s, the camera swings to 67.5° off nadir at the ends, and the wheels use 4.9 % of their capacity. The tracker is blind for 46.9 % of the pass, 34.9 % by the limb while the camera looks far along the track and 12.0 % by the Sun near the top. With the bias filter the camera holds the site within 0.1° for the whole pass, 0.026° at worst, and without the bias state for 51.15 %, 0.905° at worst. On five other seeds the bias filter again holds the whole pass, 0.023 to 0.043° at worst, and the filter without it holds 50.40 to 51.63 %.

7.6.8 A Wheel Lost Mid-Pass

Case 8 fails the roll wheel 4.5 min into the same pass, holding −0.1 % of its capacity, so its coast hands the body almost nothing. The supervisor gives roll to the coils, whose authority about roll scales with the sine of the field's angle from the roll axis. The camera passes 0.1° at 15.46 min, the field comes within 3.46° of the roll axis at 16.82 min, and the camera is 5.82° off at worst, with 81.97 % of the pass imaged. A stiffer loop ($K_p = 0.25$, $K_d = 0.9$), a softer one (0.015, 0.22), the three-axis law and perfect states all land between 81.56 and 84.75 %, and on five other seeds all five settings stay between 81.5 and 85.0 %, which is the honest infeasible case. Continuous three-axis pointing needs a torque about every axis at every instant, and with a wheel gone that depends on the field. Back at nadir two wheels and the coils hold the camera 0.013, 0.016 and 0.015° off at 30, 60 and 100 min, but with the coils busy on roll nothing unloads the others, and the pitch wheel holds 33.8 % of its capacity at 110 min, an orbit after the failure.

7.6.9 Safe Mode in the Shadow

Case 9 starts in safe mode with the arrays 63.66° off the Sun. They are within 5° of it 1.02 min later and, in sunlight, within 0.58°. The shadow lasts 34.77 min, the Sun rising at 71.2 min, and holding the gyro's reading at zero holds the true rate at minus the bias, while the drag pushes through the rate loop, so the arrays are 8.65° off the Sun at sunrise and back within 5° in 6 s. With no drag they are 6.28° off, and on five other seeds the two angles are 8.4 to 9.1° and 6.0 to 6.6°. Unloading never switches on in this case, because the excess stays under 9.7 %.

Table 7.6 The Challenge in Five Configurations at the Default Seed

Configuration	Imaged (%)	Worst (°)	Fullest (%)	Excess (%)
as shipped	24.12	27.50	100.0	100.0
unloading only	49.81	1.065	40.0	33.0
bias filter only	20.64	70.25	100.0	100.0
suggested, both	100.00	0.022	40.0	33.0
both, perfect states	100.00	0.015	40.0	33.0

Imaged within 0.1°, fullest wheel before the pass and excess at the end. Seeds 1 to 5: suggested 100 % (worst 0.021 to 0.041°), shipped 24.70 to 27.76 %, unloading only 50.06 to 53.03 %.

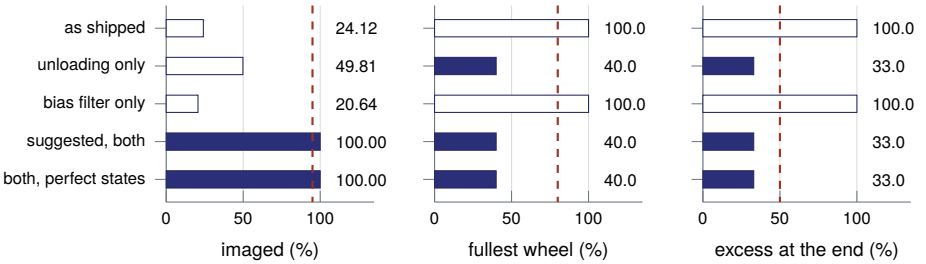


Figure 7.4 Three columns of Table 7.6 drawn as bars for the five configurations of the challenge, with its targets as dashed lines: at least 95 % of the pass imaged, no wheel past 80 % before the pass and an excess under 50 % at the end. Solid bars meet the target of their panel and white bars miss it. Notice that unloading alone passes the two momentum targets and still images only half the pass, and that the bias filter alone images less than the shipped configuration.

7.6.10 Three Orbits, Then the Pass

The challenge holds nadir for three orbits and then images Site A's pass, with unloading off and the no-bias filter as shipped. Its target asks for the true camera within 0.1° of the site for at least 95 % of the pass, no wheel past 80 % in the three orbits before it, and an excess under 50 % of a wheel when the run ends 10 min after the pass, at 302.95 min. It counts only on the case as given, so a changed model parameter or disturbance, or an extra disturbance fired, voids the attempt. At 20 simulated minutes per second the run takes about 15 s. Table 7.6 compares the configurations, and Figure 7.4 draws three of its columns as bars. As shipped the pitch wheel saturates at 245.0 min, 38.9 min before the pass, and the camera holds the site for 24.12 % of it. Each change alone fails. Unloading keeps the fullest wheel at 40.0 %, but the no-bias filter drifts through the blind half of the pass and images 49.81 %, and the bias state alone images 20.64 % because the attitude was lost before the site rose. With both the camera holds the site for the whole pass, 0.022° at worst, with the excess at 33.0 % at the end, which passes the three conditions by margins of 5, 40 and 17 percentage points, and on five other seeds the suggested configuration images 100 % each time while the shipped one images 24.70 to 27.76 %.

> **+ DID YOU KNOW? A Better Filter, a Worse Worst Moment**
>
> From the simulator: in the challenge, the gyro bias state alone leaves the camera 70.25° from the site at worst, against 27.50° with the filter as shipped. The pitch wheel still fills before the pass, so the better estimate arrives with the attitude already lost (Table 7.6).

7.6.11 A Handover Planned Inside the Limits

Case 10 flies case 7's pass and hands the camera over to Site B at 12 min, 4 min into the pass, a turn of 38.6° onto a second moving site, with the MPC pinned. Table 7.7 sets it beside the shipped laws, the eigenaxis law retuned by the MPC's own rule, once, across all of its knobs, that law fed what the

Table 7.7 The Predictive Law Against the Pointing Laws, Default Seed

Case and measure	Eigenaxis	Three axes	Retuned	Retuned, MPC signals	MPC	K_p 4, K_d 3.4
10, handover: on Site B (s), imaged (%)	52.1, 92.4	51.9, 92.5	41.9, 93.9	41.7, 94.0	**39.6, 94.3**	39.9, 94.2
10: past τ_{max} (s), torque travel (mN m)	0, 84	0, 87	0.4, 230	0.3, 236	**0**, 173	1.9, 699
10: peak relative rate (°/s)	0.999	1.335	1.002	1.002	1.015	—
10 at $J_y = 0.02$, all at 0.3: imaged (%)	80.1, 61.1	81.2, 60.9	93.6, 92.9	—	**94.2, 93.4**	94.2, 93.8
10, tracker out 11 to 17 min: on Site B (s), imaged (%)	52.2, 92.4	51.8, 92.5	42.0, 93.9	41.8, 93.9	**39.7, 94.2**	—
7: on Site A (s)	80.6	79.4	71.0	70.8	**68.7**	—
7, tracker out 10 to 16 min: worst (°), all 100 %	0.040	0.025	0.027	0.026	0.025	—
5: settled (s), peak relative rate (°/s)	102.2, 1.00	86.3, 1.73	93.1, 1.00	92.9, 1.00	**90.8**, 1.01	—
8, roll wheel fails: imaged (%), worst (°)	82.0, 5.82	**84.7, 3.63**	82.1, 5.64	82.1, 5.64	81.5, 5.74	—
3, first orbit: mean error (°), travel (mN m)	0.0188, 369	0.0188, 369	0.0077, 1008	**0.0073**, 1038	0.0076, 687	0.0070, 3199
3, three orbits: 0.1° lost (min), above 98 % (min)	250.3, 35.0	250.3, 36.6	250.3, 35.1	250.3, 38.9	250.2, 38.8	—
Challenge as shipped: imaged (%)	24.1	13.3	26.8	17.1	**28.1**	—
Challenge suggested	met	met	met	met	met	—

Retuned: the eigenaxis law with $K_p = 0.5$ (its slider's end), $K_d = 1.2$, $\omega_{lim} = 1\,^\circ/\mathrm{s}$, chosen by the MPC's own rule. MPC signals: that law with $\hat{\mathbf{d}}$ as a feedforward torque and the half-step rate correction, the strongest classical form of what the plan knows. K_p 4, K_d 3.4: the eigenaxis law past its sliders. The MPC solves 2,400 times in 20 min with no fallback, and with its preview off every row is the same to the printed digit. Travel is the summed change of the wheel commands.

plan knows, and the law past its sliders, all on the same seed, instruments and estimate. The MPC holds the camera within 0.1° of Site B 39.6 s after the handover, 1.0 s more than 38.6° takes at exactly 1 °/s, and images 94.26 % of the 11.47 min of the two passes, against 52.1 s and 92.44 % under the eigenaxis law, as shown in Figure 7.5. It spends the pitch wheel's full 3 mN m for the first second, reaches the rate limit 1.5 s after the handover, rides it at up to 1.015 °/s and brakes as late as its model allows, while the law's rate command eases out along its exponential and leaves the camera 2.90° off at 40 s.

Most of the 12.5 s is tuning, not prediction. Retuned once, the eigenaxis law settles in 41.9 s and images 93.92 %, and fed the plan's signals it settles in 41.7 s. The 2.3 s left after the retune is bandwidth that the sliders do not offer, and $K_p = 4$ with $K_d = 3.4$ closes it, 39.9 s and 94.22 %, but those gains ask the wheels for more than 3 mN m during 1.9 s of the run and move them 4.0 times as far as the plan, 699 against 173 mN m of torque travel, and 4.7 times as far over an orbit at nadir. The retuned law asks past 3 mN m for 0.4 s, and the plan never does, because the bound is a constraint of its problem. The preview is worth nothing measurable, because the reference's angular acceleration through the pass stays under 0.007 83 °/s^2 and the law's feedforward of its present value already carries it. With the preview off, every row of Table 7.7 is unchanged to the printed digit.

What the plan measurably adds is the limits, and steadiness when the spacecraft differs from its declaration. With the pitch moment at its slider's low end of 0.02 kg m^2, or every moment at 0.3 kg m^2, it images 94.22 and 93.42 % of case 10, against 93.65 and 92.89 % for the retuned law and 80.07 and 61.12 % for the eigenaxis law, which since the correction of Section 7.6.13 keeps the declared inertia just as the plan does. The stiff law images 94.24 and 93.79 % there but at $J_y = 0.02\,\mathrm{kg\,m^2}$ chatters, asking past 3 mN m for 1096 s of the 20 min and running above $1.05\omega_{lim}$ for 130.6 s.

Elsewhere the plan wins the slews and loses the failed wheel. It reaches Site A in case 7 11.9 s sooner than the law. At nadir its estimate of the drag gives the retuned law's mean error, 0.0076° against 0.0077°, with 687 against 1008 mN m of torque travel in the first orbit. Case 8 is its loss, 81.5 % imaged against 82.0 % for the law and 84.7 % for three axes. After the roll wheel fails the plan holds the coils' present authority over its horizon and cannot see the field turn toward the roll axis, so it neither saves nor spends roll authority ahead of the field's pass. The challenge as shipped saturates the pitch wheel before the pass under every law, and the plan images 28.1 % of it against 24.1 %.

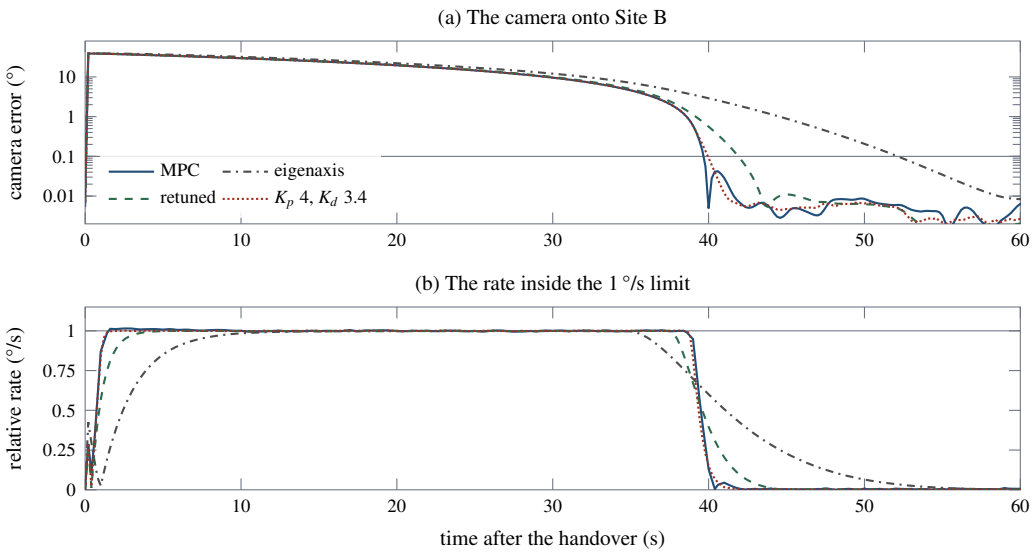


Figure 7.5 Case 10's handover to Site B under four pointing laws, on the engine with the default seed: the MPC solid, the shipped eigenaxis law dash-dotted, the law retuned by the MPC's rule ($K_p = 0.5$, $K_d = 1.2$) dashed and the stiff law ($K_p = 4$, $K_d = 3.4$) dotted. (a) The true camera error from its reference, with the 0.1° requirement as a thin gray line. (b) The true relative rate, with the 1 °/s limit as a thin gray line. The MPC and the stiff law both ride the limit and stop within 40 s, while the shipped law eases in and out and the retuned law lies between them.

7.6.12 Worst Cases Under Every Pointing Law

Every law flew every failure, outage, kick and extreme setting the application offers, as listed in Table 7.8. No run fell back, no wheel delivered more than τ_{max} or stored more than h_{max}, and dumping, safe mode, the failed axis's coils and the wheel clamps act under the MPC as under the laws. The plan is better in the torque-limited slew at 6 °/s, settled in 20.3 s against 30.8 s without asking past τ_{max}, and with a 0.5 mN m torque limit, 47.0 s against 54.5 s. It is worse at two check levels. The tracker's 1 °/s rate limit is also the slew limit the plan rides, so after a kick at nadir the tracker is blind by rate 3.2 s longer than under the law, and in the slew from wheels at 85 % 11.0 s longer, with 62.6 s over $1.02\omega_{lim}$ against 30.0 s. Every law fills a wheel in that slew. When the roll wheel fails at the handover, the plan holds the pitch command on its bound for 0.8 s of the first second and spends 3.1 s between 1.020 and 1.027 °/s on the return to nadir 7.8 min later, where the law spends none.

7.6.13 What the Review Corrected, and at What Price

A technical review of the predictive law's first build found two behaviors in which the plan was less safe than the eigenaxis law, and each was corrected and measured before and after. With one slack for the rate band over the whole horizon, a plan that started outside the box, as on the entry to nadir from detumble with a 108.8° error, paid for the excess once and rode 1.127 °/s for 14.0 s, where the law peaked at 1.001 °/s. A slack at every judged step gives 1.011 °/s and no time over $1.02\omega_{lim}$, at the price of 0.1 ms a decision, 28.1 % of the challenge imaged as shipped in place of 30.7 %, and 39.7 s in place of 39.6 s for case 10 at $J_z = 0.02\,\mathrm{kg\,m^2}$. A 20 mN m s kick, an impulse, was read by the disturbance filter as torques of 147 and 110 µN m about roll and yaw, against 2 µN m of drag, and the plan countered them with the relative rate 6 to 8 % over its limit for 39.1 s after a kick at nadir, against 5.6 s for the law. The kick test of Section 7.5.5 cuts that to 4.7 s and the tracker's rate blindness after a kick at nadir from 39.3 to 34.0 s, for 92.1 % of the pass imaged after a kick inside it

Table 7.8 Worst Cases Under Every Pointing Law, Default Seed

Case and measure	Eigenaxis	Three axes	MPC
Pitch or yaw wheel fails in the pass: %, worst °	100, 0.026	100, 0.025	100, 0.025
Roll wheel fails at the handover: s, %	52.1, 92.4	52.2, 92.4	39.6, 94.3
Tracker out the whole pass: worst °	0.040	0.039	0.038
Tracker out, no-bias filter, handover: %	0	0	0
Kick of 20 mN m s in the pass: %, s over, s blind	89.3, 5.5, 34.5	90.7, 46.0, 31.2	92.1, 4.7, 33.6
Kick at nadir: worst °, s over, s blind	0.036, 5.6, 30.8	0.018, 46.5, 47.3	0.023, 4.7, 34.0
Case 5 at 6 °/s: settled s, s past τ_{max}, peak °/s	30.8, 1.7, 5.94	34.2, 2.1, 7.66	20.3, 0, 6.00
Case 5, wheels at 85 %: settled s, s at limit, s over, s blind	111.0, 54.5, 30.0, 29.3	210.0, 181.8, 188.8, 187.3	97.0, 51.7, 62.6, 40.3
Challenge suggested, drag 10 µN m or bias 5 µT	met	met	met
Case 10, $J_x = 0.2$: s, %	52.2, 92.4	52.1, 92.4	39.7, 94.2
Case 10, $J_z = 0.02$: s, %	52.1, 92.4	52.2, 92.4	39.7, 94.2
Case 10, $\tau_{max} = 0.5$ mN m: s, %	54.5, 92.1	54.4, 92.1	47.0, 93.3
Case 2 into nadir: peak °/s, s over, s blind	1.001, 0, 1064.9	1.732, 38.1, 1094.7	1.011, 0, 1064.9
Case 9, safe mode through the shadow	safe	safe	safe

s over: true relative rate above $1.02\omega_{lim}$ in the pointing modes. s blind: tracker blind by its 1 °/s rate limit. s: time onto Site B. No fallback in any row.

in place of 92.5 %. A first form, on every innovation, slowed the slew from wheels at 85 % from 97.0 to 108.8 s, because a wheel in its fade gives real innovations up to 7.3 °/s, and was replaced.

The soft wheel ceiling stays priced with one slack, as built. Priced on every step, the $0.9h_{max}$ ceiling made the plan give up nadir at 224.8 min of case 3, 25.5 min before the law, while the wheel reached 98 % at 248.5 min anyway, so the ceiling binds only the plan's own moves.

One defect that predated the controller was fixed in the same round. The shipped laws took the run's inertia and the filters the run's tracker noise, while the plan used the declared values. All now use the declared values (Section 7.3.7), no shipped or suggested run moved, and case 10 at $J_y = 0.02\,\text{kg m}^2$ or with every moment at $0.3\,\text{kg m}^2$ falls under the eigenaxis law from 92.2 and 92.5 % imaged to 80.1 and 61.1 %.

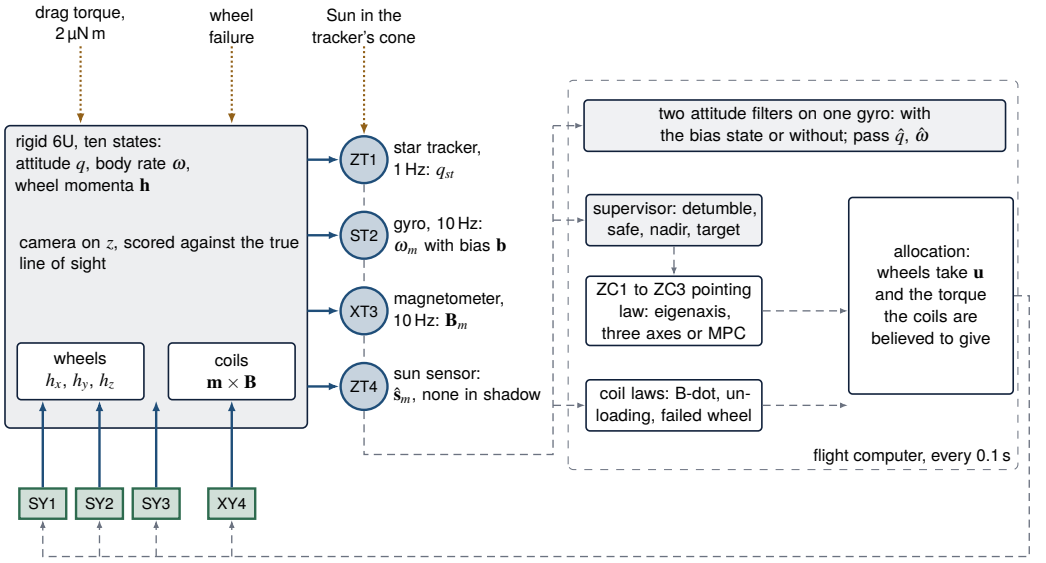
7.7 Technology in Practice

The spacecraft of Section 7.3 is read by a star tracker, a gyro, a magnetometer and a sun sensor, and moved by three reaction wheels and three coils. Figure 7.6 draws its loops with real devices in their place.

What Measures It

The tracker of Equation (7.6), with 10 arcsec of noise across its boresight and six times that about it, blind within 30° of the Sun and above 1 °/s, stands for one real star tracker. Real trackers too know the roll about the boresight less well than the boresight, and they lose their solution at a body rate that depends on the design. Missions that depend on accurate attitude carry a Kalman filter propagated on the inertial sensors to keep the attitude when the tracker loses track [23], the role of the chapter's bias filter. The magnetometer is placed well apart from the wheels, whose motors and rotors are not magnetically clean, because the coils' commands are computed from the field it measures [23]. The model assumes that the coils' own field is blanked from its readings.

> **TECHNOLOGY** **Sensor: Star Tracker**
>
> A star tracker compares a digital image of the sky with a star catalog on board and reports the full three-axis attitude, up to several times a second. The body's rate, stray light and glare can corrupt or invalidate a solution. Most modern trackers know their boresight to within a few arcseconds and the roll about it less well. A low-cost tracker may hold a solution only up to 0.3 °/s of body rate, a costlier one up to 3.0 °/s [23]. On a trend a lost solution is a gap in the tracker's readings, which a filter propagated on the gyro must bridge, as in cases 6 and 7.



SY1 to SY3: reaction wheel drives, 3 mN m and 30 mN m s each, torque fading over the last 10 % of speed; tachometers return $\mathbf{h}$ to the coil laws. XY4: three magnetorquer coils, 0.5 A m^2 each, torque only across the field.

Figure 7.6 The loops of the chapter with real devices in place of the schematic's symbols. ZT1 is the star tracker, ST2 the gyro, XT3 the magnetometer and ZT4 the sun sensor. One flight computer (dashed frame) runs the two filters, the supervisor, the pointing law on three axes (ZC1 to ZC3) and the coil laws every 0.1 s. SY1 to SY3 drive the three wheels and XY4 the three coils. Notice that the laws see only the filter's estimate and the measured field, and that only external torques such as the coils' and the drag's change the total momentum, which the wheels can store but not remove.

What Moves It

The wheels of Equation (7.4) deliver up to 3 mN m, fade over their last 10 % of speed and have no stiction near zero speed, where real wheels lose performance. Three wheels on orthogonal axes are the least that gives full three-axis control, and for a small spacecraft in Earth orbit the magnetic torquers are the main means of keeping the wheels out of saturation. A torquer is either an air coil, whose residual field dies quickly once it is switched off, or a rod with a ferrous core, which gives more dipole for the same power but can keep a residual field that upsets a magnetometer. Three torquers on orthogonal axes usually need no spare, because their windings give internal redundancy [23]. The model's coils are ideal dipoles of 0.5 A m^2 with no residual field.

> **TECHNOLOGY** **Final Element: Reaction Wheel**
>
> A reaction wheel gives torque and stores momentum along its spin axis, and the spacecraft turns the other way as the wheel speeds up. At its top speed a wheel is saturated and can neither give torque nor store more momentum in that direction, so the wheels are desaturated from time to time by an external torque from thrusters or magnetic torquers. Most wheels perform worse near zero speed, so some missions bias the wheels at half speed for finer control and less jitter, at the price of half the capacity. Static and dynamic imbalance in a wheel disturbs the spacecraft it steers [23]. On a trend saturation is a wheel momentum flat at its limit while the attitude error grows, as in case 3.

Where the Controller Runs

The chapter's flight software runs its filters, supervisor and laws on one 0.1 s step and reads the tracker once a second, where real trackers report up to several times a second. On a small spacecraft

that work is often done by an integrated attitude unit, which joins the wheels, magnetometer, torquers, sun sensors and star tracker with a processor and software for Sun tracking, inertial pointing and Earth target tracking [23], the safe, nadir and target modes of Section 7.5. The avionics of a small spacecraft are usually single-string, so one failed element can stop the whole system, and designers now add radiation-hardened or radiation-tolerant designs for long missions [23].

What Is Modernizing It

Star trackers are becoming faster, more accurate, smaller and lighter, and cheaper designs now give full three-axis attitude to missions that could not have afforded one. A magnetically levitated reaction wheel in development replaces ball bearings with active magnetic bearings to remove mechanical wear and stiction [23]. The pointing law itself can be a predictive controller that keeps the wheels' limits as constraints, as in Section 7.5.5.

> **IN PRACTICE** **Sizing the Wheels Against the Air**
>
> NASA's design criteria of 1971 for aerodynamic torques ask that the drag torque, together with every other disturbance, be shown not to degrade the attitude control. Below about 600 km aerodynamic forces usually predominate. The torque is to be computed at enough points of the orbit and times of the year to give its profile, in a model atmosphere whose density follows the sunspot cycle. The distance from the center of mass to the center of pressure is estimated conservatively large, and the result sizes the actuators' peak torque, momentum storage and momentum transfer [24].

7.8 Limitations

The spacecraft is rigid with its inertia declared to the flight software, the wheels are ideal torque sources with a linear fade, and the coils are ideal dipoles. The orbit is Keplerian apart from the node's turn, the field is the 2020 dipole without its higher harmonics, the shadow has no penumbra, and the drag torque is one constant, so the model teaches the structure of attitude control rather than the budget of a particular mission. The orbit itself, flown with drag and the Earth's oblateness, is the subject of Chapter 8.

The instruments are generic and the star tracker has no latency, stray light or acquisition time. The filter fuses the tracker alone, not the magnetometer or the sun sensor, so a long outage leaves it on the gyro, and the orbit, the time and the site are known exactly. The laws are the textbook ones, without the momentum-bias or optimal designs a mission may prefer apart from one predictive law, and every threshold of the supervisor and the scorecard is a teaching value.

The predictive law's model holds the gyroscopic torque, the coils' torque and, after a wheel failure, the coils' authority at their present values for its 60 s horizon, which is why it loses case 8. It drops the coupling of the error with the reference's rate, under 0.4 % of the torque authority at the pass's 0.86 °/s, sees the gravity gradient and the drag only through $\hat{\mathbf{d}}$, stands a soft ceiling at $0.9h_{max}$ in for the motor's fade, anticipates no switch of mode or of tasking, and leaves out the tracker's 1 °/s rate limit, which it reaches sooner than the law.

OPEN CHALLENGE Pointing on Fewer Wheels

Reaction wheel failure is a common mode of failure in many missions. A large spacecraft may carry three spare wheels, while a small one with no room for spares often mounts four wheels skewed, so that after any single failure a reduced torque remains about every axis. Magnetic torquers alone cannot usually stabilize three axes, and the coarse three-axis pointing shown with them in research takes several orbits and an orbit inclined enough for the field to vary [23]. In case 8 two wheels and the coils image at most 84.75 % of the pass in every tuning tried. Progress would be laws that plan the coils' authority as the field turns.

7.9 Conclusion

On this simulator a 6U CubeSat points a camera with wheels that store every torque they absorb, coils that act only across a turning field and a filter that coasts on a biased gyro, and the camera is scored against a truth the flight software never sees. A drag torque of 2 µN m fills the pitch wheel by 37.85 % an orbit and costs the attitude at 245.0 min. The coils empty a 78.1 % excess in 58.6 min while up to 84 % of it lies out of their reach, and over an orbit they remove an excess along the orbit normal twice as fast as one in the plane. B-dot is fastest near 0.5 mN m s and three times slower at 8. The eigenaxis law flies a 90.45° slew through 90.62° where three separate axes fly 105.28°. Without the bias state the camera drifts 2.35° in the Sun's blind window, and a failed wheel caps a pass at 84.75 % in every tuning tried. The challenge rises from 24.12 % of the pass imaged to 100 % only with both unloading and the bias state. The model omits flexibility, the field's higher harmonics and solar pressure, and a fuller model would add a momentum-biased design, a star tracker with latency and stray light, a filter that fuses the field and the Sun, and unloading scheduled around the passes. The spacecraft is a browser laboratory for actuators that keep what they apply, and its optional predictive law shows that a plan's measured gain on a handover, 39.6 against 52.1 s, comes from staying inside the wheels' limits at full bandwidth rather than from looking ahead.

KEY POINTS

- A wheel turns the spacecraft by spinning the other way, so it stores every torque it absorbs, and only the coils, pushing across the Earth's field, can empty it.
- A drag torque of 2 µN m fills the pitch wheel by 37.85 % an orbit and costs the attitude at 245.0 min.
- B-dot is fastest near 0.5 mN m s and three times slower at 8, because a strong law leaves the body turning about the field line.
- The challenge rises from 24.12 % of the pass imaged to 100 % only with both unloading and the bias state.

Where else this applies. Volume 4, Chapter 13 meets the same limit in feet that push only inside a friction cone, and Volume 5, Chapter 13 drifts between position fixes as this filter drifts between star tracker readings.

References

[1] J. Puig-Suari, C. Turner, and W. Ahlgren, "Development of the standard CubeSat deployer and a CubeSat class PicoSatellite," in *2001 IEEE Aerospace Conference Proceedings*, vol. 1, 2001, pp. 347–353.

[2] I. Ofodile, J. Kütt, J. Kivastik, M. Kaspar Nigol, A. Parelo, E. Ilbis, H. Ehrpais, and A. Slavinskis, "ESTCube-2 attitude determination and control: Step towards interplanetary CubeSats," in *2019 IEEE Aerospace Conference*, 2019, pp. 1–12.

[3] F. L. Markley and J. L. Crassidis, *Fundamentals of Spacecraft Attitude Determination and Control*, ser. Space Technology Library. New York, NY: Springer, 2014.

[4] National Aeronautics and Space Administration, "Spacecraft magnetic torques," National Aeronautics and Space Administration, Washington, DC, Space Vehicle Design Criteria (Guidance and Control) NASA SP-8018, Mar. 1969. [Online]. Available: https://ntrs.nasa.gov/citations/19690020961

[5] P. J. Camillo and F. L. Markley, "Orbit-averaged behavior of magnetic control laws for momentum unloading," *Journal of Guidance and Control*, vol. 3, no. 6, pp. 563–568, 1980.

[6] A. Astolfi and M. Lovera, "Global spacecraft attitude control using magnetic actuators," in *Proceedings of the 2002 American Control Conference*, vol. 2, 2002, pp. 1331–1335.

[7] G. Avanzini and F. Giulietti, "Magnetic detumbling of a rigid spacecraft," *Journal of Guidance, Control, and Dynamics*, vol. 35, no. 4, pp. 1326–1334, 2012.

[8] E. J. Lefferts, F. L. Markley, and M. D. Shuster, "Kalman filtering for spacecraft attitude estimation," *Journal of Guidance, Control, and Dynamics*, vol. 5, no. 5, pp. 417–429, 1982.

[9] F. L. Markley, "Attitude error representations for Kalman filtering," *Journal of Guidance, Control, and Dynamics*, vol. 26, no. 2, pp. 311–317, 2003.

[10] R. E. Fischell, "Magnetic and gravity attitude stabilization of Earth satellites," Applied Physics Laboratory, The Johns Hopkins University, Report AD0271383, Defense Technical Information Center, May 1961.

[11] J. R. Wertz, Ed., *Spacecraft Attitude Determination and Control*, ser. Astrophysics and Space Science Library. Dordrecht: D. Reidel, 1978.

[12] E. Y. Yu, "Spin decay, spin-precession damping, and spin-axis drift of the Telstar satellite," *Bell System Technical Journal*, vol. 42, no. 5, pp. 2169–2193, 1963.

[13] A. C. Stickler and K. T. Alfriend, "Elementary magnetic attitude control system," *Journal of Spacecraft and Rockets*, vol. 13, no. 5, pp. 282–287, 1976.

[14] B. Wie and P. M. Barba, "Quaternion feedback for spacecraft large angle maneuvers," *Journal of Guidance, Control, and Dynamics*, vol. 8, no. 3, pp. 360–365, 1985.

[15] B. Wie, H. Weiss, and A. Arapostathis, "Quaternion feedback regulator for spacecraft eigenaxis rotations," *Journal of Guidance, Control, and Dynamics*, vol. 12, no. 3, pp. 375–380, 1989.

[16] C. C. Liebe, "Accuracy performance of star trackers - a tutorial," *IEEE Transactions on Aerospace and Electronic Systems*, vol. 38, no. 2, pp. 587–599, 2002.

[17] J. E. Van Cleve, S. B. Howell, J. C. Smith, B. D. Clarke, S. E. Thompson, S. T. Bryson, M. N. Lund, R. Handberg, and W. J. Chaplin, "That's how we roll: The NASA K2 mission science products and their performance metrics," *Publications of the Astronomical Society of the Pacific*, vol. 128, no. 965, p. 075002, 2016.

[18] P. Alken, E. Thébault, C. D. Beggan *et al.*, "International Geomagnetic Reference Field: the thirteenth generation," *Earth, Planets and Space*, vol. 73, p. 49, 2021.

[19] D. Q. Mayne, J. B. Rawlings, C. V. Rao, and P. O. M. Scokaert, "Constrained model predictive control: Stability and optimality," *Automatica*, vol. 36, no. 6, pp. 789–814, 2000.

[20] Ø. Hegrenæs, J. T. Gravdahl, and P. Tøndel, "Spacecraft attitude control using explicit model predictive control," *Automatica*, vol. 41, no. 12, pp. 2107–2114, 2005.

[21] U. Eren, A. Prach, B. B. Koçer, S. V. Raković, E. Kayacan, and B. Açıkmeşe, "Model predictive control in aerospace systems: Current state and opportunities," *Journal of Guidance, Control, and Dynamics*, vol. 40, no. 7, pp. 1541–1566, 2017.

[22] G. Pannocchia and J. B. Rawlings, "Disturbance models for offset-free model-predictive control," *AIChE Journal*, vol. 49, no. 2, pp. 426–437, 2003.

[23] S. V. Weston, C. D. Burkhard, J. M. Stupl, R. L. Ticknor, B. D. Yost, R. A. Austin, P. Galchenko, L. K. Newman, and L. Santos Soto, "State-of-the-art small spacecraft technology," National Aeronautics and Space Administration, Ames Research Center, Moffett Field, CA, Technical Publication NASA/TP-20250000142, Jan. 2025. [Online]. Available: https://ntrs.nasa.gov/citations/20250000142

[24] National Aeronautics and Space Administration, "Spacecraft aerodynamic torques," National Aeronautics and Space Administration, Washington, DC, Space Vehicle Design Criteria (Guidance and Control) NASA SP-8058, Jan. 1971. [Online]. Available: https://ntrs.nasa.gov/citations/19710016459

7.10 Exercises

7.1 ⌕ Concept check · 2 min

In scenario 3 the camera holds nadir to 0.018° on average for more than two orbits, and then, at 245.0 min, the attitude is lost although no setting has changed. What is the cause?

(a) The pointing gains are too low to resist the drag torque once the pitch wheel spins fast

(b) The pitch wheel has stored the drag's momentum orbit after orbit and, near its capacity, can absorb no more torque

(c) The gravity-gradient torque grows with the pitch wheel's speed until it overpowers the pointing law

(d) The bias estimate of the filter drifts over three orbits until the estimated attitude is no longer trusted

7.2 Concept check · 2 min

In scenario 2 the B-dot law detumbles the spacecraft from 10.1 °/s. With a gain of 0.5 mN m s the rate falls under 0.5 °/s in 26.8 min, and with 8 mN m s in 85.5 min. Why is the stronger law slower?

(a) The larger dipoles saturate the magnetometer, so the law loses its measurement of the field's rate

(b) The larger gain makes the filter on the field's rate unstable, so the dipoles chatter

(c) The strong law quickly removes the rate across the field and leaves the body turning about the field line, where the coils make no torque

(d) The larger dipoles add a torque along the field that spins the body up again

7.3 Concept check · 2 min

In scenario 5 both pointing laws use the same gains and the same 1 °/s slew rate limit to make a change of attitude of 90.45°. The eigenaxis law turns the body through 90.62° at up to 0.94 °/s. The three-axis law turns it through 105.28° at up to 1.69 °/s. Which explanation is right?

(a) The three-axis law applies higher gains on the axis with the largest error, so it overshoots

(b) The three-axis law leaves out the gyroscopic term, so the body is pushed off its path

(c) The three Euler angles cannot describe a rotation this large, so the three-axis law mistakes the error

(d) Each loop limits only its own component, so the rate vector can reach nearly $\sqrt{3}$ times the limit along a direction off the eigenaxis

7.4 Theory and calculation · 5 min

The spacecraft holds nadir with unloading off. A drag torque of 2 µN m, fixed in the body about pitch, acts the whole time. The orbit's mean motion is $n = 1.106\,783 \times 10^{-3}\,\mathrm{rad/s}$, a wheel holds at most $h_{max} = 30\,\mathrm{mN\,m\,s}$, and each coil's dipole is limited to $0.5\,\mathrm{A\,m^2}$.

(a) Find the orbital period and the momentum the pitch wheel gains in one orbit, as a share of its capacity. *Checkpoint:* 5677 s (94.62 min) and 37.85 %.

(b) Find the time from an empty wheel to 98 % of capacity, in orbits and in minutes. *Checkpoint:* 2.59 orbits, 245.0 min.

(c) The field along the orbit runs from 23.69 to 47.37 µT. Find the largest torque one coil at its limit can make across it, and the torque the unloading law asks with $\tau_d = 15\,\mathrm{min}$ at the 40 % excess that switches it on. *Checkpoint:* 11.8 to 23.7 µN m, and 13.3 µN m.

7.5 Theory and calculation · 6 min

Over the first three orbits the orbit average of $\hat{\mathbf{b}}\hat{\mathbf{b}}^{\mathsf{T}}$, the field's direction times itself, is diag(0.493, 0.491, 0.016) in the axes $(\hat{\mathbf{P}}, \hat{\mathbf{Q}}, \hat{\mathbf{h}})$ of Equation (7.8). The unloading law runs with $\tau_d = 15\,\mathrm{min}$ and no dead band.

(a) Find the time constant with which an excess along the orbit normal decays, and the time constants of an excess along $\hat{\mathbf{P}}$ and along $\hat{\mathbf{Q}}$. *Checkpoint:* 15.24 min, and 29.59 and 29.47 min.

(b) Find the time each excess takes to fall to a tenth, and compare with the engine's 36.2, 70.3 and 64.4 min for the pitch, yaw and roll excess, which start along $\hat{\mathbf{h}}$, $-\hat{\mathbf{P}}$ and $\hat{\mathbf{Q}}$. *Checkpoint:* 35.1, 68.1 and 67.9 min.

(c) Explain why the drag's excess at nadir is the easiest one to unload, and why an excess in the orbit plane falls in steps. *Checkpoint:* The field lies close to the orbit plane.

7.6 Theory and calculation · 6 min

The pointing law of Equation (7.11) runs with $K_p = 0.0625/\mathrm{s}^2$, $K_d = 0.45/\mathrm{s}$ and $\omega_{lim} = 1\,^\circ/\mathrm{s}$.

(a) Find the natural frequency and the damping ratio of the unsaturated loop. *Checkpoint:* 0.25 rad/s and 0.9.

(b) Find the error angle below which the rate command leaves its limit, for the shipped gains and for the gains $K_p = 0.5$, $K_d = 1.2$ that the MPC's tuning rule chose for the eigenaxis law. *Checkpoint:* 7.2° and 2.4°.

(c) Case 10 hands the camera over to a site 38.6° away. Find the shortest time any law held to the rate limit could take, and the largest body rate three single-axis loops held to the same limit could reach. *Checkpoint:* 38.6 s and 1.73 °/s.

7.7 App challenge · 8 min

Load scenario 3, Nadir hold: the wheels creep, and change no setting. Run at 20 simulated minutes per second to 285 min, three orbits, with the default seed, and export the CSV file. The file's time column is in hours.

(a) Read the pitch wheel's momentum, column `hy_abs_pct`, in the row nearest one orbit, 94.62 min. *Checkpoint:* 37.84 %, within 0.05 %.

(b) Find the first row in which `hy_abs_pct` reaches 98 %, and the first row in which the camera's true error, column `point_err_deg`, exceeds 1°. Give both times in minutes. *Checkpoint:* 245.0 min and 250.8 min, each within 0.1 min.

(c) Press the reload button, set Momentum dumping On on the MOM card before Run, and run again to 285 min. Read the Fullest wheel tile. *Checkpoint:* 40.0 % (pitch).

Compare (a) and (b) with the drag's budget $\tau_a T / h_{max}$.

7.8 App challenge · 8 min

Load scenario 6, The gyro bias and the blind window, as shipped, with the Attitude estimate at EKF, no bias. Run to 27 min at 1 simulated minute per second with the default seed and export the CSV file, whose time column is in minutes. The column `tracker_blind` is 1 while the star tracker reports nothing, and `point_err_deg` is the camera's true error.

(a) Find the row in which the tracker goes blind, the row in which it reports again, and the largest `point_err_deg` between them. *Checkpoint:* 14.08 to 25.58 min, and 2.34°, within 0.05°.

(b) Press Reset, set the Attitude estimate to EKF + bias before Run, and repeat. *Checkpoint:* 14.08 to 24.92 min, and 0.054°, within 0.005°.

(c) The true gyro bias is 7, −9 and 5 °/h about roll, pitch and yaw. Estimate the drift of the no-bias filter's attitude across the camera axis over the window of (a), and explain why that window is longer. *Checkpoint:* About 2.2°.

7.9 App challenge · 9 min

Load the challenge, Challenge: three orbits, then the pass. Use the default seed and let each run end by itself at 302.95 min, at 20 simulated minutes per second. After each run read the Pass imaged, Fullest wheel and Excess momentum now tiles.

(a) Run the challenge as shipped, with unloading off and the Attitude estimate at EKF, no bias. *Checkpoint:* 24.1 %, 100.0 % and 100.0 %.

(b) Press Reset, set Momentum dumping On and run. Then press the reload button, set the Attitude estimate to EKF + bias and run. *Checkpoint:* 49.8 %, 40.0 and 33.0 %, then 20.6 %, 100.0 and 100.0 %.

(c) Press Reset, set Momentum dumping On as well and run. *Checkpoint:* 100.0 %, 40.0 and 33.0 %.

Explain why each change alone fails the target.

7.10 Application area · 4 min

The drag torque at nadir follows the air density, which changes by several times over a solar cycle. The app's drag slider reaches 10 µN m. Use $T = 5677\,\mathrm{s}$, $h_{max} = 30\,\mathrm{mN\,m\,s}$ and $\tau_d = 15\,\mathrm{min}$.

(a) With unloading off, find the momentum the pitch wheel gains per orbit and the time from an empty wheel to 98 %. *Checkpoint:* 189.2 % of capacity, 49.0 min.

(b) With unloading on all the time, the excess along the orbit normal settles where the averaged law's torque equals the drag. Find that excess and say what it means for the dead band of 40 and 10 %. Name two changes that would add margin. *Checkpoint:* About 30.5 % of a wheel.

7.11 Application area · 3 min

In case 8 the roll wheel fails during the pass, and the coils take over roll. Their roll torque is $\mathbf{m} \cdot (\mathbf{B} \times \hat{\mathbf{x}})$, and the field comes within 3.46° of the roll axis at 16.82 min.

(a) With a dipole of $0.5\,\mathrm{A\,m^2}$ along $\mathbf{B} \times \hat{\mathbf{x}}$ and a field of 23.69 to 47.37 µT, find the largest roll torque at that instant, and compare it with a wheel's 3 mN m. *Checkpoint:* 0.71 to 1.43 µN m, about 2100 to 4200 times less.

(b) Name two ways an operator could keep imaging with two wheels. *Checkpoint:* Plan passes and attitudes around the field.

7.12 Review the agent · 5 min

An AI assistant reviews scenario 10 and writes: "The MPC puts the camera on Site B in 39.6 s against 52.1 s for the eigenaxis law because its 60 s preview of the site's path lets it brake at the right moment. Prediction is what the classical law lacks. Switch every pass, and the challenge as shipped, to the MPC with its preview on, and the same gain will follow." Find the flaw and say how you would check it on the app.